

Spring 5-13-2017

A Study in Cross-Beam Polarization Fluorescence Photoactivation Localization Microscopy on Dendra2-Hemagglutinin in Fixed NIH3T3 Cells

Matthew M. Valles

University of Maine, matthew.valles@maine.edu

Follow this and additional works at: <http://digitalcommons.library.umaine.edu/etd>



Part of the [Biological and Chemical Physics Commons](#)

Recommended Citation

Valles, Matthew M., "A Study in Cross-Beam Polarization Fluorescence Photoactivation Localization Microscopy on Dendra2-Hemagglutinin in Fixed NIH3T3 Cells" (2017). *Electronic Theses and Dissertations*. 2672.
<http://digitalcommons.library.umaine.edu/etd/2672>

This Open-Access Thesis is brought to you for free and open access by DigitalCommons@UMaine. It has been accepted for inclusion in Electronic Theses and Dissertations by an authorized administrator of DigitalCommons@UMaine.

**A STUDY IN CROSS-BEAM POLARIZATION FLUORESCENCE PHOTOACTIVATION LOCALIZATION
MICROSCOPY ON DENDRA2-HEMAGLUTTININ IN FIXED NIH3T3 CELLS**

By Matthew Mandell Valles

B.S. Bates College, 2013

A THESIS

Submitted in Partial Fulfillment of the

Requirements for the Degree of

Master of Science

(in Physics)

The Graduate School

The University of Maine

May 2017

Advisory Committee:

Samuel T. Hess, Professor of Physics, Advisor

Raymond D. Astumian, Professor of Physics

John R. Thompson, Professor of Physics

© 2017 Matthew M. Valles
All rights reserved

**A STUDY IN CROSS-BEAM POLARIZATION FLUORESCENCE PHOTOACTIVATION LOCALIZATION
MICROSCOPY ON DENDRA2-HEMAGLUTININ IN FIXED NIH3T3 CELLS**

By Matthew M. Valles

Thesis Advisor: Dr. Samuel T. Hess

An Abstract of the Thesis Presented
in Partial Fulfillment of the Requirements for the
Degree of Master of Science
(in Physics)
May 2017

Fluorescence microscopy is popular for its noninvasive properties and its use in imaging multiple species, simultaneously. Furthermore, superresolution fluorescence microscopy (SRFLM) utilizes photoswitchable proteins to improve the lateral resolution of conventional fluorescence microscopy by an order of magnitude. There is little work conducted on the study of excitation laser polarizations and their effect on the number of localizations as well as the brightness of molecules. This thesis attempts to study the effect of excitation wavelength polarization on the number of localizations and the brightness of molecules by comparing two orientations of circularly-polarized, excitation lasers. The first type of orientation involves collinear excitation beams perpendicular to the sample stage (widefield). The second involves two, crossed excitation beams so that they overlap only at the area imaged in a sample (cross-beam).

Dendra 2-HA is the fluorescent protein Dendra2 tagged to the influenza virus protein hemagglutinin. The fluorescent protein is commonly used in studies related to the spread of the influenza virus in mammalian cells, such as NIH3T3 cells. With equal excitation rates

between the two beam orientations, the cross-beam, with 73 degrees between the beams, yielded more localizations and more narrow brightness histograms than that of the widefield variety. Simulation results show a similar trend, but are not analytically in agreement with those of the experimental variety. Maximization of the number of localizations combined with minimization of the brightness histogram widths can be achieved with ninety degrees between the beams and equal excitation rates, per the simulation. This result suggests that the cross-beam orientation has the potential to be of use in the improvement of multiple fluorescent species superresolution studies.

ACKNOWLEDGEMENTS

I am very grateful to Dr. Sam T. Hess for providing me with this great opportunity to learn and grow as a biophysicist over these past few years. His patient guidance and support has been invaluable. This work would not have been possible without him.

I would also like to acknowledge members of my committee, Drs. John Thompson and Raymond Dean Astumian. Their support and helpful questions guided my research in such a way that they helped me to understand better the various parts of the project, and how they fitted together. They also helped me to better understand and explain how the research fits in with others that are like this one.

Many thanks, I give, to fellow physics students of the undergraduate, graduate and post-graduate variety. These include but are not limited to Drs. Nikki Curthoys, Andrew J. Nelson and Michael Mlodzianoski, Matthew Parent, Michael Brady Butler, Eric Breitbach, Prakash Raut, Shawn Brackett, Jacquelin Wallace and Logan Boyd. I greatly appreciate the many helpful conversations, guidance, support and help in the Bennett Hall of Physics and Astronomy.

I also express my gratitude for my counselor at the Cutler Health Center, Dr. Amy Moran, students at the Catholic Newman Center, especially Kevin McFadden, FOCUS missionaries and my spiritual director Fr. Bill Labbe. The emotional and spiritual support that these and others provided were invaluable for this work.

Finally, I thank Mom, Dad and my brother, William, for providing me with the means to receive an education such as this. Without their support, this would not have been possible.

Vivat Jesus!

TABLE OF CONTENTS

ACKNOWLEDGEMENTS	iii
LIST OF TABLES	vi
LIST OF FIGURES.....	vii
CHAPTER 1 INTRODUCTION	1
1.1. Fluorescence Microscopy Resolution	1
1.2. Circumventing the Diffraction Barrier	2
1.3. FPALM Concept	3
1.4. A desire for more localizations, distinguishing features	5
1.5. Cross-beam FPALM in membrane studies	9
CHAPTER 2 FPALM METHODS	10
2.1. Sample Preparation	10
2.1.1. Cell maintenance	11
2.1.2. Subculture	11
2.1.3. Transient transfection	12
2.1.4. Cell Fixation	12
2.2. FPALM imaging and analysis	13
2.2.1. Laser path	13
2.2.2. Fluorescence collection	16
2.2.3. Laser profile and intensity	16
2.2.4. Image acquisition	17
2.2.5. Localization precision	17

2.2.6. Cross-beam analysis	18
2.2.7. Rendering	19
2.2.8. Simulation of Gaussian area method	20
CHAPTER 3 RESULTS	23
3.1. Excitation rates	23
3.2. Experimental number of photon histograms	26
3.2.1. Both circularly polarized beams	30
CHAPTER 4 DISCUSSION	32
4.1. Maximum number of localizations and photon counts	32
4.2. Fluorophore selection based on polarization, number of photons emitted	33
4.3. Simulation results do not agree with those of the experiment	34
4.3.1. Blinking	38
4.3.2. Non-uniformities in the beam intensity	40
4.3.3. Laser incident polarizations	40
4.3.4. Transition dipole orientations.....	41
4.4. Future directions	41
4.4.1. Multicolor imaging	47
4.4.2. Single color multispecies imaging	49
4.4.3. Mitigating emitted photon variation due to blinking	52
REFERENCES	54
APPENDIX SUPPORTING INFORMATION	58
BIOGRAPHY OF THE AUTHOR	86

LIST OF TABLES

Table 3.1. Background noises.....	27
Table 3.2. Experimental A , S and x_0 values	28
Table 4.1. A , S and x_0 simulation values with experimental angles and excitation rates.....	34

LIST OF FIGURES

Figure 1.1. The concept of FPALM	4
Figure 1.2. The properties of excitation rate	6
Figure 1.3. The effect of beam polarization on various transition dipoles	8
Figure 1.4 The effect of cross-beam polarization on various transition dipoles	9
Figure 2.1. Basic layout of an FPALM set-up	13
Figure 2.2. A view of the cross-beam orientation with the excitation lasers	14
Figure 3.1. Normalized excitation and emission spectra	23
Figure 3.2. 561 and 532 nm beam profiles	24
Figure 3.3. A rendered image of Dendra 2-HA in an NIH3T3 cell	25
Figure 3.4. Experimental number of photons per localization per frame	26
Figure 3.5. Average photon full width at half maxima	30
Figure 4.1. Simulation histograms, experimental parameters	35
Figure 4.2. Simulation and experiment average full width at half maxima	36
Figure 4.3. Simulation model	37
Figure 4.4. Experimental blinking for 694 localizations	38
Figure 4.5. Simulation histograms, ideal parameters	41
Figure 4.6. Simulated average FWHM, ideal parameters	43
Figure 4.7. TIRF with rotation diagram	45
Figure 4.8. Lipid raft model	47
Figure 4.9. A multicolor imaging detection path with cross-beam orientation	48
Figure 4.10. Simulation of Dendra2 and lipophilic Dil number of photon histograms	49

Figure 4.11. Normalized fluorescence emission spectra of DiO, DiI, DiD, and DiR bound to phospholipid bilayer membranes	50
Figure A.1. Single cell photon histograms	84

CHAPTER 1

INTRODUCTION¹

1.1. Fluorescence Microscopy Resolution

Fluorescence microscopy is a popular imaging technique both for its relatively noninvasive properties and its ability to simultaneously image multiple species in living cellular specimens. The technique is relatively non-invasive, capable of providing single molecule labeling specificity, and compatible with the imaging of living specimens (Hell et al. 2007). Images are formed by the simultaneous observation of many fluorescing molecules to visualize cellular structures and processes.

In conventional far-field fluorescence microscopy, the spatial resolution is diffraction-limited. This is because the wave-like nature of light causes diffraction, which prevents the focusing of a beam into a spot substantially smaller than half a wavelength in size (Gould et al. 2012). The image of an object, in far-field fluorescence microscopy, is a superposition of point sources. Each point source has a shape given by the point spread function (PSF), whose size is given by $r_0 \sim 0.47\lambda/NA$, where r_0 is the $1/e^2$ radius, λ is the wavelength of the detected light and NA is the numerical aperture of the microscope lens.

Distinct identification of point sources is possible when they are separated by a distance greater than r_0 . In most biological samples, however, tens of thousands of labeled species can reside in an area of radius r_0 , so are not possible to resolve in conventional fluorescent light microscopy. Thus, the smallest resolvable details are given by the Rayleigh criterion, namely

$$R_0 \geq \frac{0.61\lambda}{NA}$$

where R_0 is the distance between point sources, λ is the wavelength of the photons detected and NA is the numerical aperture of the lens system (Born and Wolf 1997). Two point-like emitters must have a separation greater than R_0 to be distinguishable. In far-field fluorescence light microscopy, a typical lateral resolution is ~ 200 nm, which is greater than the size of many labeled species in a biological sample.

1.2. Circumventing the Diffraction Barrier

Many important biological processes occur on length scales shorter than the diffraction limit, and the motivation to improve optical resolution in fluorescence microscopy has been strong. Fortunately, one can observe these phenomena through the use of localization-based super resolution techniques: Stochastic Optical Reconstruction Microscopy (STORM) (Rust et al. 2006), Photoactivatable Localization Microscopy (PALM) (Betzig et al. 2006), and Fluorescence Photoactivation Localization Microscopy (FPALM) (Hess et al. 2006). These and related techniques have recently become quite popular. These were the first localization-based super-resolution techniques, obtaining lateral resolutions of 20-30 nm, or slightly less. The techniques make use of probe photophysics to control the transition between on and off states that provide one with the means to optically resolve subsets of fluorophores in each time. Those that make use of STORM imaging utilize a photoswitchable probe that consists of two distinct conventional organic dyes, which can reversibly cycle between bright and dark states in the presence of a reducing agent such as thiol (Bates et al. 2005). FPALM and PALM utilize photoactivatable fluorescent proteins (PA-FPs) that initially reside in a non-fluorescent metastable state and switch to a fluorescent form upon irradiations with an activation laser, usually by ultraviolet or near ultraviolet light. This allows for precise localization of each

emitter. Eric Betzig, inventor of PALM, Stefan W. Hell, and William E. Moerner, received the 2014 Nobel Prize in chemistry for their contributions to super resolution microscopy in biological imaging (Nobel Media AB, 2014).

1.3. FPALM Concept

Localization microscopy is made possible by labeling samples with specific fluorescent molecules that can be converted from a dark to bright state and eventually to another dark (bleached) state (Fig. 1). Within the sample, an activation laser is used to potentiate the fluorescence of small subsets of single molecules. A second, and sometimes even a third, readout laser excites the fluorescence of those molecules so that they are imaged as diffraction-limited point-spread functions (PSFs) (Fig. 1 A-C). During imaging, or, more typically after imaging, the molecular images are then mathematically analyzed to determine the two- or three-dimensional coordinates of each identified molecule, which is called localization (Fig. 1 E-G). One controls the molecular activation and bleaching rates to allow only a small number of molecules to be visible at once, and to cause those molecules to be separated by a distance greater than R_0 . Two dimensional plots of this information constitute the image (Fig. 1). Localization microscopy can improve the diffraction-limited resolution by about a factor of 10 or more (Fig. 1 D, K). This enables the elucidation of biological structures on sub-diffraction length scales.

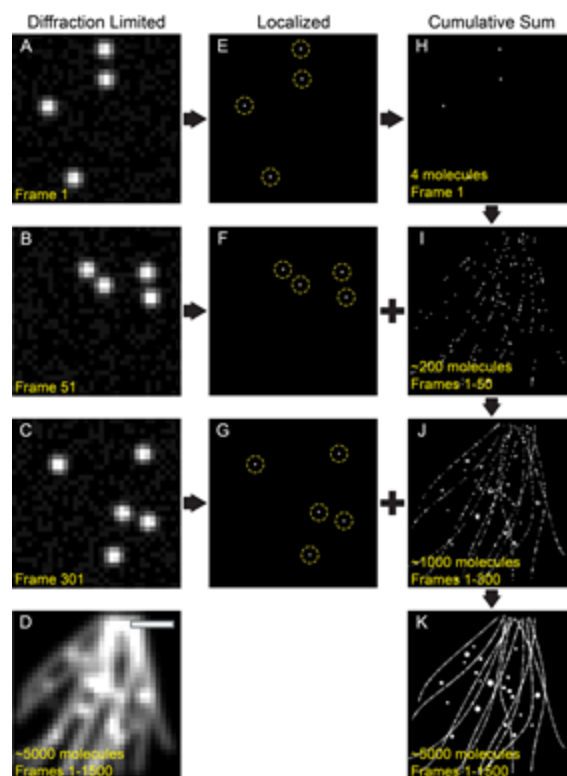


Figure 1.1: The concept of FPALM. The simulated concept of FPALM shows diffraction-limited single molecules that are sparsely activated, excited, and imaged before they photobleach (A). Photobleached molecules are replaced in each frame by newly activated single molecules (B,C). Together, all of the single molecules form a diffraction limited image (D). The recorded single molecules in (A-C) are mathematically localized (E-G, enclosed in yellow circles). The cumulative sum of the localized molecules form super resolved images (H-K). Sparse numbers of molecules (H,I) do not adequately define the structures as well as larger numbers of molecules (J,K). Scale bar in (D) is 1 μm and is the same for all images.

Localization microscopy can image individual fluorophores as well as multiple fluorophores simultaneously (Bossi et al. 2008, Testa et al. 2010, Gunewardene et al. 2011). Molecular orientations, and localizations in two or three dimensions (Juetten et al. 2008, Huang et al. 2007), can also be determined. Super resolution imaging can be performed in live cells (Hess et al. 2007, Shim et al. 2012) and fixed samples. Fixed cell imaging reveals static information about the size and spatial organization of the labeled structures at one instant in time. Live cell imaging reveals dynamics of cellular structures and enables the measurement of

single molecule trajectories on millisecond timescales (Gudheti et al., 2013, Manley et al., 2008).

1.4. A desire for more localizations, distinguishing features

One desires to see more molecules sample with little variation in the number of photons emitted by each fluorophore (Mlodzianoski et al. 2016). This is because one is only able to see a small subset of molecules in each sample, through conventional FPALM methods. Molecular orientations have been studied via the use of FPALM with membranes (Gould et al. 2008), but there is still a need to control laser polarization to excite and localize a larger subset of molecules in a given sample and to optimize their distribution of emission rates for quantification of molecular properties.

Fluorophores emit light as transition dipoles via the following relationship,

$$k_x = k_{x0} \cos^2(\theta)$$

where k_x is the excitation rate of the transition dipole, k_{x0} is the maximum excitation rate and θ is the angle between the excitation light polarization and transition dipole (Lakowicz 2006).

An important aspect of the equation above is the angle between the light incident onto the sample with the transition dipole orientation. In each sample, molecules can have different orientations such that their excitations differ from one another when linearly polarized light is incident onto the sample. With circularly polarized light, one has the means to excite all transition dipole orientations in a plane, given that the photons are energetically able to cause the transition. Molecules with transition dipole orientations that are either partially or totally out of the circularly polarized light plane will have excitation rates less than the ones that do not have this feature. It is therefore desirable to increase the excitation rates for those

molecules with transition dipoles that are not in the same plane as the incident circularly polarized light.

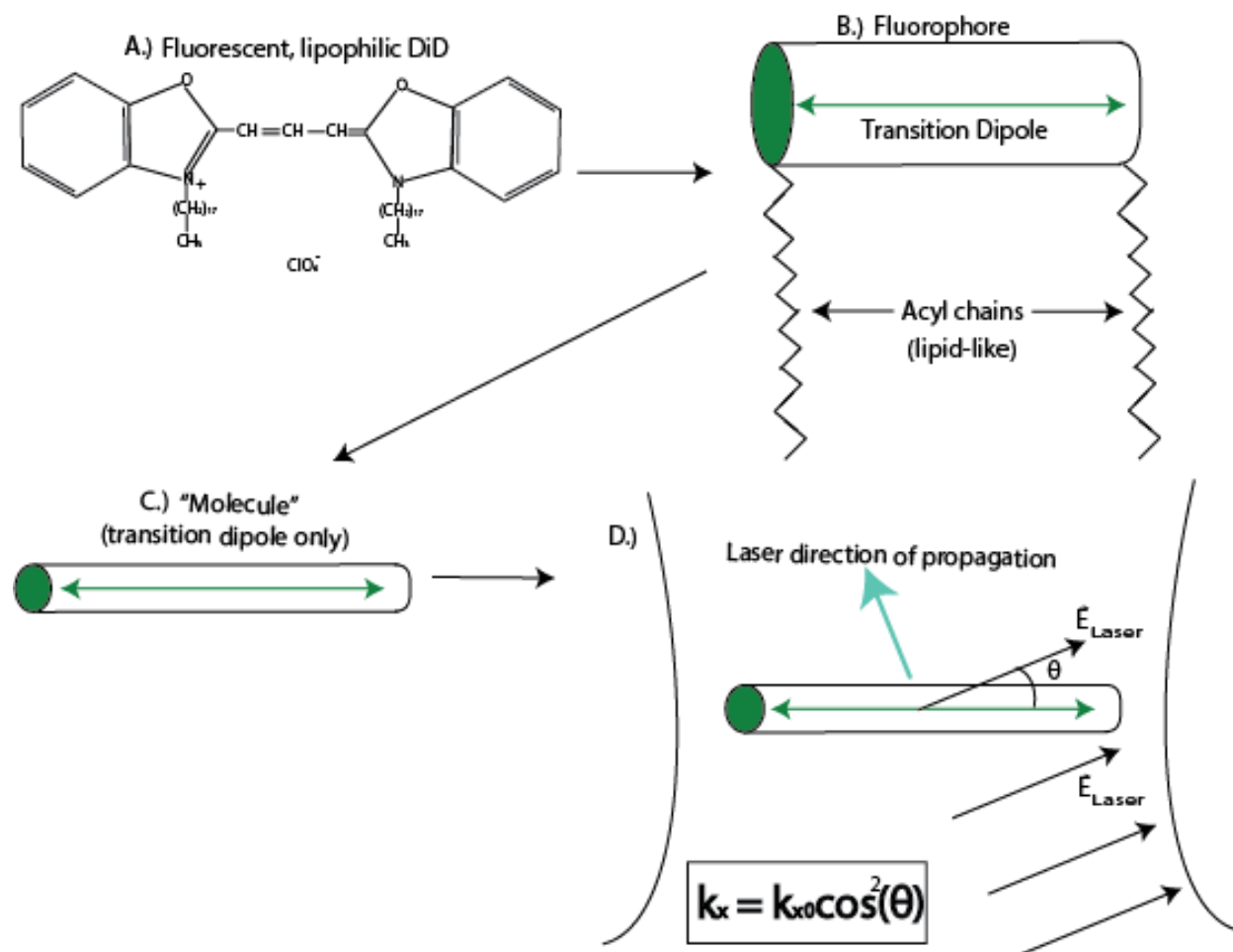


Figure 1.2: The properties of excitation rate. The excitation rate properties of DiD, which is a dye that attaches to lipids, show the principle that governs whether a fluorophore emits. A.) Lipophilic DiD fluorescence is such that electrons transition along the plane of the molecule. B.) As a fluorophore, DiD can be viewed as a cylinder with a transition dipole within it that has acyl chains, which attach to lipids. C.) The DiD molecule is present with great emphasis on the transition dipole only. D.) The DiD molecule is present with its transition dipole oriented at an angle θ with respect to the electric field of the laser, \vec{E}_{Laser} . This causes the excitation rate to be $k_x = k_{x0} \cos^2(\theta)$, where k_{x0} is the maximum excitation rate.

One way to excite more transition dipoles that are not in the same plane as circularly polarized widefield incident light (Figure 1.3 roman numeral I) is to use tilted illumination of

one laser (Figure 1.3 roman numeral II). In this type of orientation, one has the means to excite all molecules in a plane that is at some angle less than ninety degrees from the coverslip-sample interface. In this way, one can excite more transition dipoles that cannot be excited with the circularly polarized, widefield, incident light. However, there is still a plane perpendicular to this orientation that does not have the opportunity to be excited as shown in Figure 1.3.

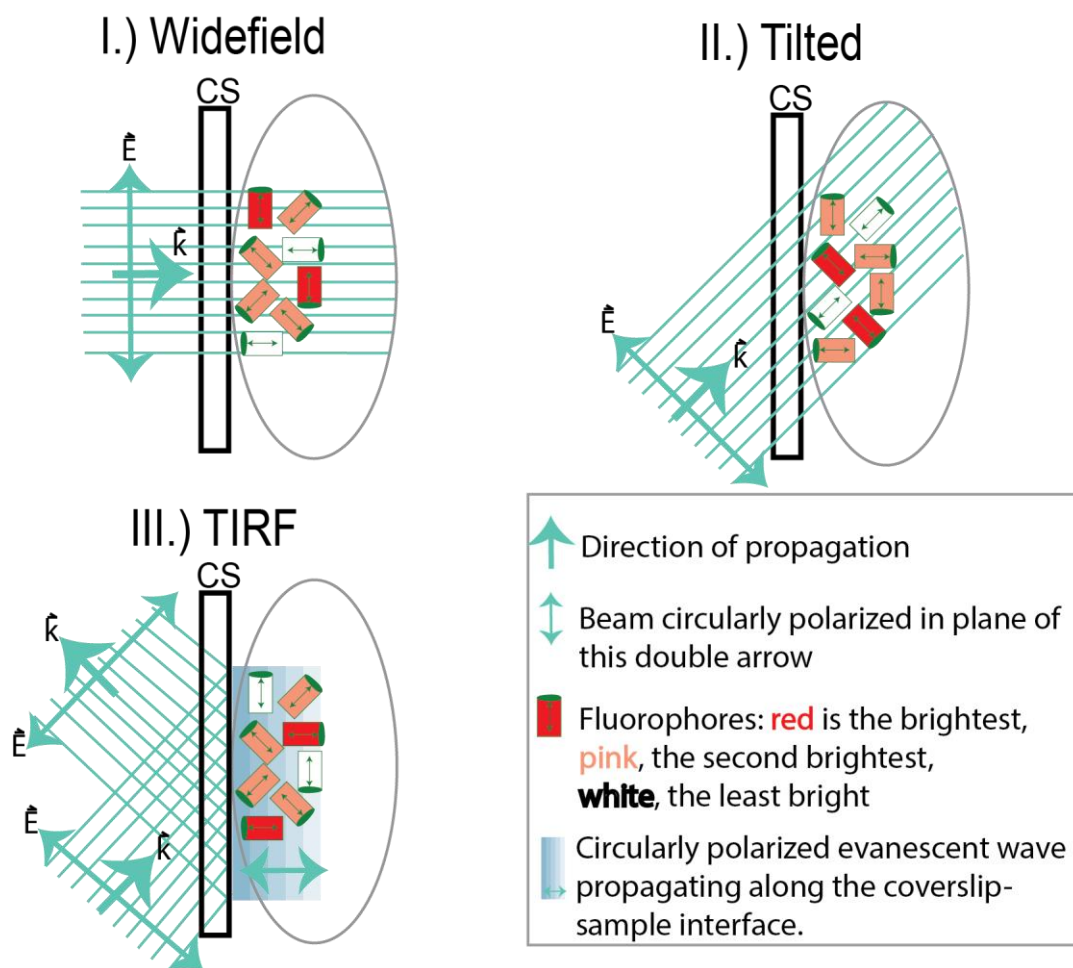


Figure 1.3: The effect of beam polarization on various transition dipoles. The effects of beam polarization on various transition dipoles that can be excited show that circularly-polarized beams cannot excite all transition dipoles. The beams are all circularly polarized, and vary in their incident polarizations based on the illumination type. The transition dipoles shown in the diagram are excited based on their orientation with respect to the incident beam, dependent on the relationship, $k_x = k_{x0} \cos^2(\theta)$, described in chapter 1.4. I.) Widefield, II.) Tilted and III.) TIRF illuminations are shown in the diagram above. No one of these illuminations has the potential to excite transition dipoles of all possible orientations in each sample. Vectors \vec{k} and \vec{E} are the propagation direction and electric field vectors, respectively.

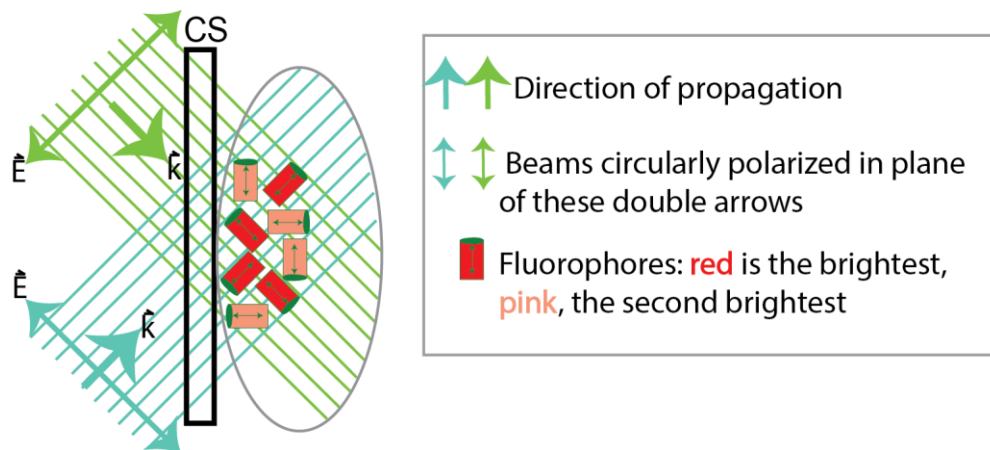
Another way to increase the excitation rate of transition dipoles that are not in the same plane as circularly polarized, widefield, incident light (Figure 1.3 roman numeral I) is to use total internal reflection fluorescence (TIRF). In this type of orientation, excitation laser light totally internally reflects off the interface between the coverslip and sample to send an

evanescent wave along the plane where these two mediums meet (Figure 1.3 roman numeral III). If the light is circularly polarized, then one of the polarization directions remains the same while the other takes on an orientation perpendicular to that of the plane where the coverslip and sample meet. In this way, the linear combination of polarizations can excite all those transition dipoles in a plane perpendicular to that of the interface between the coverslip and sample. If more molecules are oriented in this way than in the plane interface between the coverslip and sample, then one can achieve more localizations with TIRF than with the widefield orientation. However, in all the illumination types shown in figure 1.3, there is present the chance that not all fluorophores will be excited, unless their transition dipoles are all oriented parallel to one plane or another.

1.5. Cross-beam FPALM in membrane studies

The use of two, wavelength-distinct excitation beams allows for the possibility of orienting each one to be at an angle, ninety degrees or less, with respect to each other such that both can excite all orientations of transition dipoles in different planes. The linear combination of the transition dipoles in the two planes allows for all possible excitation orientations to be accessible. Furthermore, if the excitation rates for the two beams are similar, then there will be more dipoles that send out similar photons in each time than those accessed in the widefield, circularly polarized light orientation. This is because the beams oriented at an angle ninety degrees or less with respect to one another can access all orientations of dipoles such that the angle between the fluorophores and the electric field of the laser is never 90 degrees, and can often be close to zero degrees. For the widefield orientation, the angle between the transition dipoles is not necessarily zero because some of

the dipoles can be oriented outside of the plane through which the beam passes. Thus, the transition dipoles in the beams that cross one another at an angle should be more distinguishable than those accessed via a circularly-polarized, widefield, TIRF and tilted illumination beams because the excitation rate should be constant as a function of angle between the beam and transition dipole.



IV.) Cross circular-circular

Figure 1.4: The effect of cross-beam polarization on various transition dipoles. The effect of IV.) Cross-beam polarization on various transition dipoles shows that the illumination has the potential to excite all transition dipole orientations in each sample.

CHAPTER 2

FPALM METHODS

2.1. Sample preparation

Preparation of samples can follow standard protocols for fluorescence labeling, however several crucial details need to be considered. Photoactivatable single molecules, by nature, are sensitive to light. Once labeled, samples should be shielded from stray light sources (room lights, incubator UV, etc) which may prematurely activate single molecules. Additionally, sample media and buffers often contain auto-fluorescent components that serve to increase background noise and worsen the localization precision. Sample media and buffers should be made such that auto-fluorescent components are removed or replaced with non-fluorescent alternatives.

2.1.1. Cell maintenance

NIH3T3 cells (Sigma-Aldrich) were maintained at a less than 100% confluent monolayer in a T25 flask (Sigma-Aldrich) in Dulbecco's modified eagle's medium (Thermo Fisher Scientific) supplemented with 10% calf bovine serum (ATCC), 0.45% weight per volume (w/v) glucose and 0.15% (w/v) sodium bicarbonate with phenol red and antibiotics. The incubator was maintained at 37 degrees Celsius and 5% CO₂.

2.1.2. Subculture

Cells between 70 and 90% confluency were washed with 1 mL of 0.05% Trypsin-EDTA and subsequently incubated for 5 minutes. After the cells detached, the cell suspension was added to 5 mL of Dulbecco's modified eagle's medium (Thermo Fisher Scientific) supplemented

with 10% calf bovine serum (ATCC), 0.45% weight per volume (w/v) glucose and 0.15% (w/v) sodium bicarbonate with phenol red and antibiotics. The solution was then pipetted so as to wash off cell clumps from the flask's side before a thirty times pipetting minimized clumping in the corner of said flask. 100,000 cells were seeded into a new T25 flask with 5 mL of Dulbecco's modified eagle's medium (Thermo Fisher Scientific) supplemented with 10% calf bovine serum (ATCC), 0.45% weight per volume (w/v) glucose and 0.15% (w/v) sodium bicarbonate with phenol red and antibiotics.

2.1.3. Transient transfection

NIH3T3 fibroblast cells were plated at 20,000 cells per well incubated between twelve and thirty hours at 37 degrees Celsius and 5% CO₂ in eight-well chambers with a #1.5 coverslip bottom (Labtek II, Nalge-Nunc International Corp.). Each well contained the cells in 0.5 mL of Dulbecco's modified eagle's medium (Thermo Fisher Scientific) supplemented with 10% calf bovine serum (ATCC), 0.45% weight per volume (w/v) glucose and 0.15% (w/v) sodium bicarbonate without phenol red or antibiotics. Cells were transfected with ~1 µg per well of Dendra2-HA using Lipofectamine 3000 reagents (Thermo Fisher Scientific) in Opti-MEM reduced-serum media (Thermo Fisher Scientific) without antibiotics according to the manufacturer's directions. The nunc was then wrapped in aluminum foil and then incubated at 37 degrees Celsius and 5% CO₂ for an additional 24-30 hours.

2.1.4. Cell Fixation

After the 24-30 hour wait period, cells were removed from the incubator, rinsed three times in UV-bleached phosphate buffer solution (PBS), incubated for ~30 minutes in 4%

paraformaldehyde (Sigma-Aldrich) in PBS at room temperature, and rinsed three more times with UV-bleached PBS. These were imaged within two weeks of fixation. The cells were stored in a four degrees Celsius refrigerator until they were imaged.

2.2. FPALM imaging and analysis

2.2.1 Laser path

For various functionalities, the microscope can be aligned to match one of the possible layouts in Figure 2.1. The activation laser, which frequently has a 405 nm wavelength, was adjusted to spatially overlap with the readout laser[s] at the coverslip. The readout wavelength[s] can be one or several different wavelengths, chosen to best excite the fluorescent molecules in the sample. Readout laser 1 is the 561 nm diode laser (Laserglow Technologies, Toronto, ON), readout laser 2 is the 532 nm diode laser (Sapphire, Coherent, Santa Clara, CA) and the 405 nm diode laser is the activation laser (Crystalaser, Reno, NV). All three lasers are typically focused by a lens into the back aperture of the objective to achieve widefield illumination at the sample, as shown in panel I of Figure 2.1. In this kind of illumination, the path of the laser lies directly on the optical axis, which results in excitation through the sample. By shifting the path of the laser laterally away from the optical axis, the laser beam becomes inclined in the sample, as seen in panel II. Further shifting of the laser from the optical axis puts the excitation into total internal reflection fluorescence (TIRF) mode, as seen in panel III. In TIRF, the evanescent electric field penetrates only a few hundred nanometers into the sample, enabling excitation of only molecules very close to the surface of the coverslip and greatly reducing out of focus background.

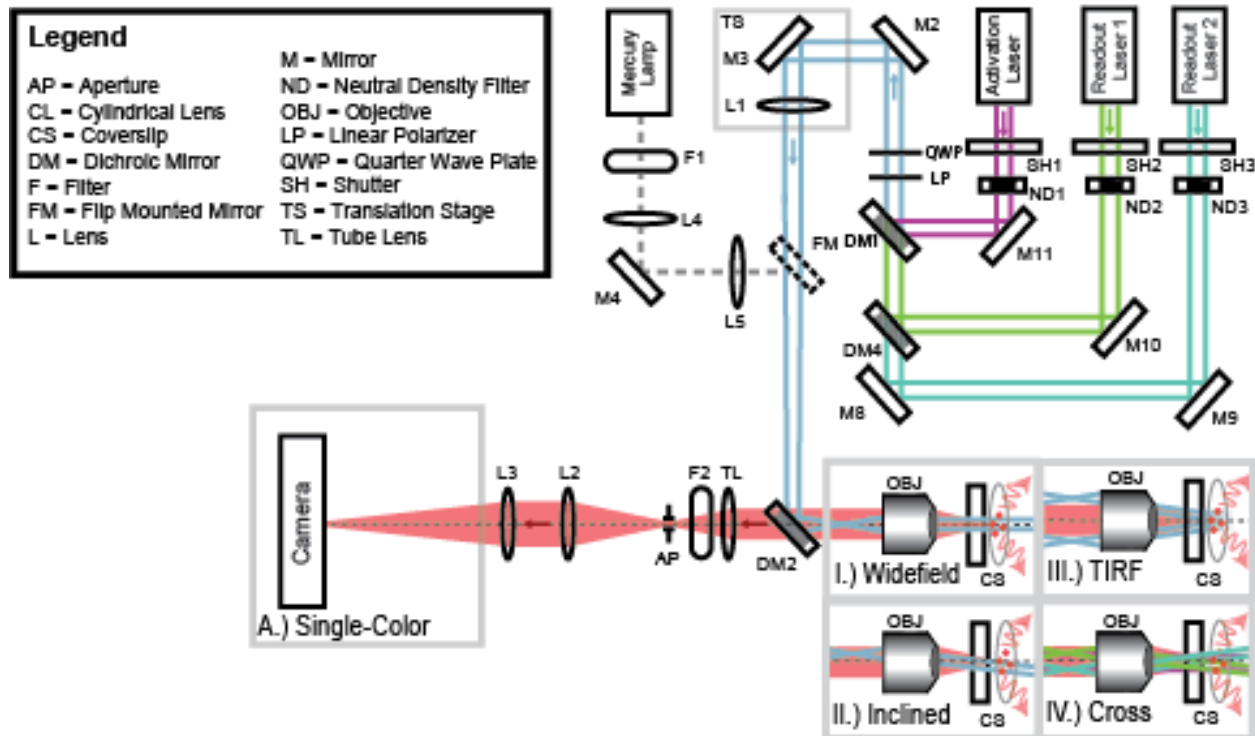


Figure 2.1: Basic layout of an FPALM set-up. Basic layout of an FPALM setup and many modifications. The Readout 1, Readout 2 and Activation laser on/off and powers are controlled by shutters, SH, and neutral density filters, ND, respectively. The lasers are combined at DM1 and reflected to the lens, L1, by mirrors M2 and M3. The lasers pass through a linear polarizer, LP, quarter wave plate, QWP, for conversion to circularly polarized light, then reflect off the filter cube dichroic, DM2, and focus at the back aperture of the objective, OBJ. The lateral position of the lasers at the back aperture of the objective controls the angle at which the lasers enter the sample; I.) centered for excitation perpendicular to the coverslip, II.) slightly offset for inclined beam in the sample, and III.) offset for total internal reflection fluorescence (TIRF). The lateral position of the laser is adjusted by shifting the translation stage, TS. Sample fluorescence is collected by the objective, passes through DM2, and is focused by the tube lens, TL. Outside the microscope, additional bandpass filters, F2, remove background. The aperture, AP, reduces the image region. The image is expanded by the telescope lenses, L2 and L3 before entering the detection box. Modifications to the detection path enable different modes of imaging. For single color imaging, fluorescence is measured directly by the camera (A). For simultaneous multi-color imaging, a dichroic, DM3, separates the fluorescence into two channels (B). Light from the Mercury Lamp passes through a filter, F1, and expands with the telescope lenses L4 and L5. A flip mirror, FM, reflects the mercury lamp light into the microscope.

Panel IV of Figure 2.1 results from a process known as walking the beam, where the two mirrors in the beam paths of Readout Lasers 1 and 2 (M8 and M9 as well as M10 and DM4) were used to put their beams into inclined illumination. This was done by laterally adjusting the angles of the beams from M8 and M10 before correcting the position of these beams at the coverslip via the use of M9 and DM4. The result is shown in Figure 2.2. Figure 2.2A.) shows the beams with one representing 561 nm and the other, 532 nm. Figure 2.2B.) shows a close-up view of the circularly polarized beams intersecting at the sample, just to the right of the coverslip. As shown in Figure 2.2, the inclined illumination of both beams is such that they do not cross anywhere else, but at the sample with the activation laser.

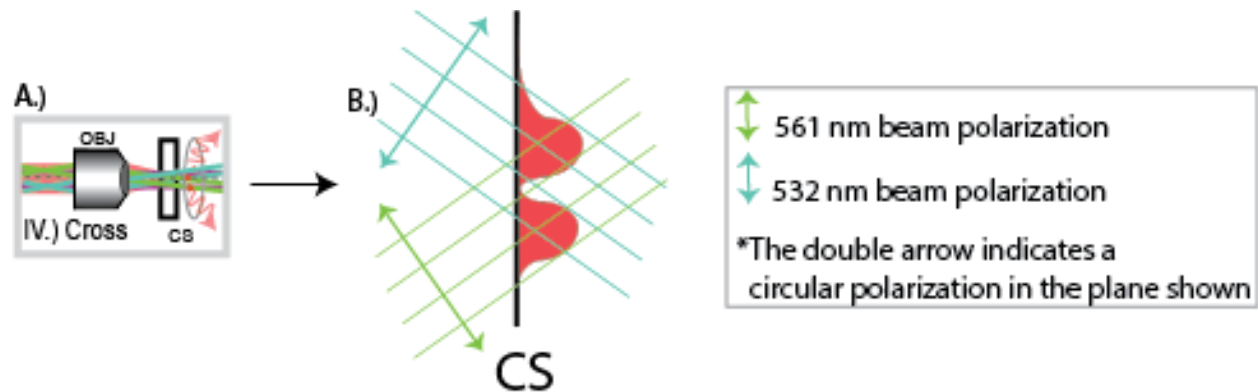


Figure 2.2: A view of the cross-beam orientation with the excitation lasers. A view of the cross-beam orientation with the excitation lasers, colors that more closely resemble 561 and 532 nm light, that were used in experiments (A). A magnified view of the cross-beam excitation is such that the lasers are circularly polarized and incident on to the sample shown by the red, Gaussian-looking structures to the right of the CS (B). The activation laser is in a widefield orientation shown in A.), but not in B.).

2.2.2 Fluorescence collection

The lens behind the back port of the inverted microscope (IX 71, Olympus) had a focal length of +350 millimeters. The distance between the lens and the back aperture of the objective lens (PLAPO 60XO3TIRFM, Olympus, Melville, NY) was the focal length of the lens used for the experiments. Zeiss Immersion 518F (Carl Zeiss Microscopy, Thornwood, NY) was used as immersion oil for the objective lens, which collects a portion of the excited fluorescence. This fluorescence then passed through a dichroic, Z565LP (Chroma, Bellow Falls, VT), emission filter LP561RU (Semrock, Rochester, NY), as well as a tube lens that formed an image in an intermediate plane. At the intermediate plane, an aperture (SM1D12D, Thorlabs, Newton, NJ) restricted the region of interest around the imaging area, which had a diameter $\sim 10\text{ }\mu\text{m}$. Notch filters NF03-405E-25, NF03-532E-25, and NF03-561E-25 (Semrock, Rochester, NY) were used to further eliminate the laser light from the detection path. This image was recorded with an Andor iXon EM-CCD camera (DU-897 DCS-BV, Andor Technology, South Windsor, CT) that provided two-dimensional spatial information.

2.2.3. Laser profile and intensity

The readout laser powers were controlled by a manual neutral density filter wheel (Newport, Irvine, CA) so that the excitation rates were made to be as similar as possible for the two beams incident onto the sample of Dendra 2-HA in NIH3T3 cells. The activation laser power was controlled by a set of a manual and computer controlled neutral density filter wheel coupled to a LabView (National Instruments, Austin, TX) program so that its power was $1.5\text{ }\mu\text{W}$

or less. The profile of each laser was imaged with a set of autofluorescent filter slides (Chroma, Bellow Falls, VT).

2.2.4. Image acquisition

Point-spread function (PSF) images of individual photoactivatable fluorescent proteins (PA-FPs) were acquired using Andor Solis software (Andor Technology, South Windsor, CT) bundled with the EMCCD camera. For each fixed cell in the cross-beam experiments, 10,000 frames of 9.5 ms exposure time were acquired at a rate of 88.97 Hz, an EM gain of 200 and a pre-amplifier gain of 5.2. To image each live cell in the Lipid DiD and Dendra 2-HA experiments, everything was the same except that the frame rate was 44 Hz, the exposure time was 20.54 ms and the pre-amplifier gain was 4.2. Images were saved in an uncompressed, stacked TIFF format and subsequently analyzed by a localization program written in MATLAB, called Einzel.

2.2.5. Localization precision

The rolling ball algorithm was used to subtract region-specific background away. This was done to smooth the original image to yield local values of the background. A rolling ball radius of 6 pixels smoothed the images themselves. Images were subtracted for region-specific background using the rolling ball algorithm where the original image is smoothed to yield local values of the background.

PSFs of fluorescing PA-FPs were identified by scanning for pixel values above a certain threshold consistent for the experiments of a given day. 7 pixel-by-7 pixel areas containing the center of the PSFs were fitted with a two-dimensional Gaussian via the use of the least-square method to determine the localized two-dimensional coordinates, amplitude, radius as well as vertical offset. The number of photons was calculated by multiplying the amplitude of the

fitted Gaussian by its area. The localization precision, σ_{xy} , was determined by using the equation,

$$\sigma_{xy}^2 = \frac{s^2 + q^2}{N} + \frac{8\pi s^4 b^2}{q^2 N^2}$$

where N is the number of photons, s , the standard deviation of the PSF, q , the pixel size at the sample plane and b , the background noise in photons per pixel (Thompson et al., 2002).

The same background noise value of the equation above was used for all localizations in an acquisition. The standard deviation of the detected photons (noise) the root of the mean number because it is Poisson-distributed. Thus, the background noise of the channel was determined by selecting a representative area close to, but not including, a PSF in the channel. The PSFs localized were further tolerated based on the number of photons, N , $1/e^2$ radius r_0 , as well as the two-dimensional fitting uncertainties.

2.2.6. Cross-beam analysis

A crucial part of the cross-beam experiment analysis involved calculating the brightness of each localization in each sample of Dendra2-HA in a NIH3T3 mouse fibroblast. Localization brightness histograms were generated to observe trends related to photophysics of Dendra2 in a cell membrane. To calculate the brightness of each localization, we used a Gaussian area method. This method made use of the number of photons for a localization's brightest pixel, a_0 , $1/e^2$ area of the PSF of the point spread function, πr_0^2 , where the area is in units of pixels squared. The brightness in number of photons, N , was calculated as follows:

$$N = \frac{a_0 \pi r_0^2}{2}$$

This is because the localizations emit photons so that this spatial emission is modeled by a Gaussian distribution so that N is equal to the area under the Gaussian distribution.

Trajectory analysis was run on the Einzel-analyzed files to gather information about fluorophores that emitted photons for three or more frames. Localizations found in three or more successive frames to be within seventy nanometers of the localization in the previous frame of each other were selected. After these localizations were selected, the first and last frame information was discarded, as it showed parts of the emission that did not involve the whole exposure time of a frame. A given molecule begins emitting light at some point during the exposure time of the first frame and ceases to emit at some point in time during the last frame. Thus, the middle frame information for an emission was used for analysis because the localizations emitted for the full duration of these frames.

After discarding the first and last frame emissions for each trajectory, information regarding location of the emission with respect to the center of mass for the localizations as well as that of the number of photons per localization were retained. From this information, histograms were made showing the number of events versus either the localization distance from the center of mass or number of photons per trajectory per frame. These were calculated by the Gaussian area method.

2.2.7. Rendering

Each localized molecule was rendered to display them as intensity-weighted Gaussians of a prescribed size imprinted on a magnified image. Dendra2 molecules were rendered as green.

2.2.8. Simulation of Gaussian area method

In the cross-beam experiments, simulations were developed to examine more closely the theory behind the experimental phenomena. The theory behind the simulation involves fluorescence quantum yields as well as considerations related to dipole orientations with respect to incident laser polarizations. The simulation provides an estimate for the number of photons from a single species of fluorescent molecules, and does not account for saturation effects (Gould et al. 2009).

In the simulation, the number of a uniform distribution of molecular transition dipoles equaled that of the experimental findings. The transition dipoles were made to be oriented between 0 and 180° with respect to a plane of interest. Next, the transition dipoles were placed randomly in a circular area, consistent with that of the experiment. The equation below demonstrates the placement of the transition dipoles in the experiment:

$$r_p = A * (X^2 + Y^2)^{0.5} \quad (1)$$

The variable, r_p , is the distance between the center of mass and the transition, X and Y are a set of random numbers generated between 0 and 1. The quantity of the random numbers between 0 and 1 equals that of the number of particles found experimentally in the system. The variable A is approximately equal to the distance in microns between the center of mass and the position where many of the particles were found.

After simulating uniformly-distributed, randomly-placed transition dipoles, a simulation of the two beams incident onto this sample was developed. This was done via the use of

equations related to the excitation rates of the two beams. A Gaussian beam's $1/e^2$ radius in centimeters, ω_0 , is used with the power in Watts, P , to calculate the intensity, I_0 :

$$I_0 = \frac{2 * P}{\pi \omega_0^2} \quad (2)$$

The energy per photon, $E_{\text{photon},\lambda}$, was also calculated via the use of the equation below with the wavelength in nanometers λ_{nm} :

$$E_{\text{photon},\lambda} = \frac{2\pi(197.3 \text{ eV} \cdot \text{nm})}{\lambda_{nm}} * 1.602 * 10^{-19} \frac{J}{eV} \quad (3)$$

Along with the energy per photon and beam intensity, the excitation cross-section, σ_λ , was determined for one beam incident onto a sample with a fluorophore using the extinction coefficient, ε_λ , in units of $(\text{cm} * M)^{-1}$ as shown below:

$$\sigma_\lambda = \varepsilon_\lambda * 3.82 * 10^{-21} \quad (4)$$

Equation (1-4) comes from the Beer-Lambert equation (Lakowicz 2006), and has units of centimeters squared. The equation was used to calculate the excitation rate, $k_{x\lambda}$, of one laser beam incident onto a sample with a fluorophore:

$$k_{x\lambda} = \frac{I_0}{E_{\text{photon},\lambda}} * \sigma_\lambda * e^{\frac{-2r_p^2}{\omega_0^2}} \quad (5)$$

The total excitation rate, $k_{x\text{total}}$, for two beams combined and incident onto a sample; with some angle, θ , between the direction of propagation of $k_{x\lambda 1}$ and the transition dipole

orientations; as well as some angle α between directions of propagation for the two beams is as follows:

$$k_{xtotal} = k_{x\lambda 1} \sin^2(\theta) + k_{x\lambda 2} \sin^2(\theta + \alpha) \quad (6)$$

The number of photons detected per localization per frame, N , is determined via the use of the quantum yield, φ_{fl} , time per frame, τ_{frame} , detection efficiency, φ_{det} , and the total excitation rate:

$$N = k_{xtotal} \varphi_{fl} \tau_{frame} \varphi_{det} \quad (7)$$

Simulated number of photon histograms are in chapter three to compare with those of the experimental variety.

CHAPTER 3

RESULTS

3.1. Excitation rates

In the cross-beam and widefield excitations, there was the desire to make the excitation rates of the 561 and 532 nm lasers different only by the angle between the beams. The maximum excitation rate, k_{x0} , is as follows,

$$k_{x0} = \sigma I$$

with $\sigma = 3.82 * 10^{-21} * \varepsilon$, where σ is the excitation cross-section and ε is the extinction coefficient in $M^{-1}cm^{-1}$. For Dendra2, $\varepsilon = 35000 M^{-1}cm^{-1}$ at the peak excitation wavelength of 553 nm (Gould et al., 2009). For the excitation laser 532 nm and 561 nm wavelengths, activated normalized fluorescences are 0.609 and 0.816, respectively. Thus, their extinction coefficients for Dendra2 are $21,308 M^{-1}cm^{-1}$ and $28,560 M^{-1}cm^{-1}$.

The intensity, I , is as follows,

$$I = \frac{P \lambda_{nm} * 5.04 * 10^{15} \frac{photons}{s}}{\pi w_0^2}$$

with P as the beam power in Watts, λ_{nm} , the wavelength in nanometers, $5.04 * 10^{15} \frac{photons}{s}$, the number of photons per second clarified by a quantum theory of radiation processes, πw_0^2 , the $1/e^2$ area of the beam in cm^2 .

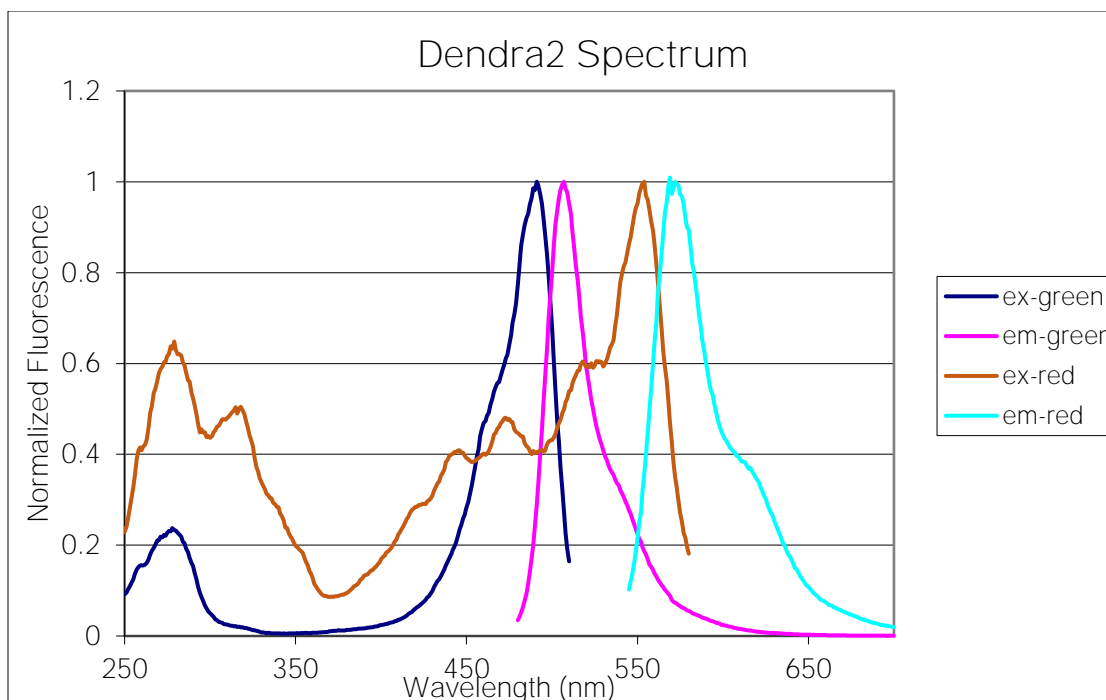


Figure 3.1: Normalized excitation and emission spectra. Normalized excitation lines demonstrate the non-activated (ex-red and em-red) as well as activated (ex-green and em-green) spectra (Gurskaya et al. 2006).

With the beam profiles and scale image shown in Figure 3.2, the $1/e^2$ radii and areas were calculated. Thus, the excitation rates for the 561 and 532 nm beams were calculated by measuring the power of the beams via the use of a power meter (PM100D Thorlabs, Newton, NJ), before dividing this by the $1/e^2$ area of the beam, which was calculated by using the program of Appendix Supporting Information 1. For the beams shown in Figure 3.2, the excitation rates are equal when the 532 nm power is 14.0 mW while the 561 nm power is 10.2 mW. Experimentally, the 561 nm beam was adjusted to match the excitation rate of the 532 nm beam. This was to make their functionality similar in the excitation of fluorophores.

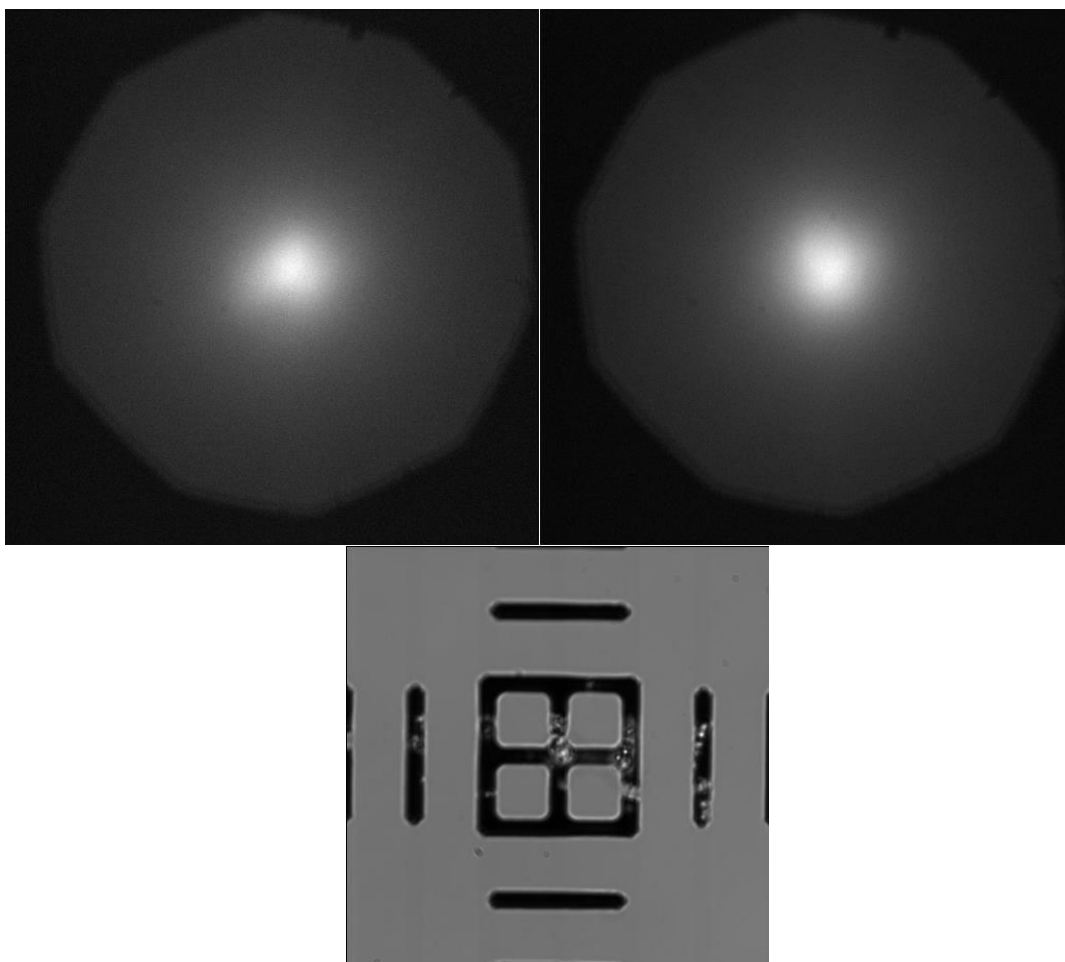


Figure 3.2: 561 and 532 nm beam profiles. Beam profiles for the 561 (top left) and 532 (top right) nm lasers as seen at the sample stage in $\sim 10 \mu\text{M}$ solution of Rhodamine B (Sigma-Aldrich, Austin, TX). The $1/e^2$ areas of the two beams are $3.65 * 10^{-6} \text{cm}^2$ and $3.45 * 10^{-6} \text{cm}^2$, respectively. The calculation of the $1/e^2$ radii and pixel size were made via the use of the computer programs shown in Appendices A.1 and A.2, respectively, as well as an image of the scale (bottom middle). The distance between the dashes in the scale image is ten microns.

The 532 and 561 nm lasers were used with the 405 nm activation laser on NIH3T3 fibroblasts that had Dendra2-HA within them. Below is a rendered image of the Dendra2-HA in a NIH3T3 fibroblast, on the left, and on the right is a transmitted light image. The edge where the very black and grey pixels' meet is the edge of the aperture closed around the cell as well as some space outside of the cell.

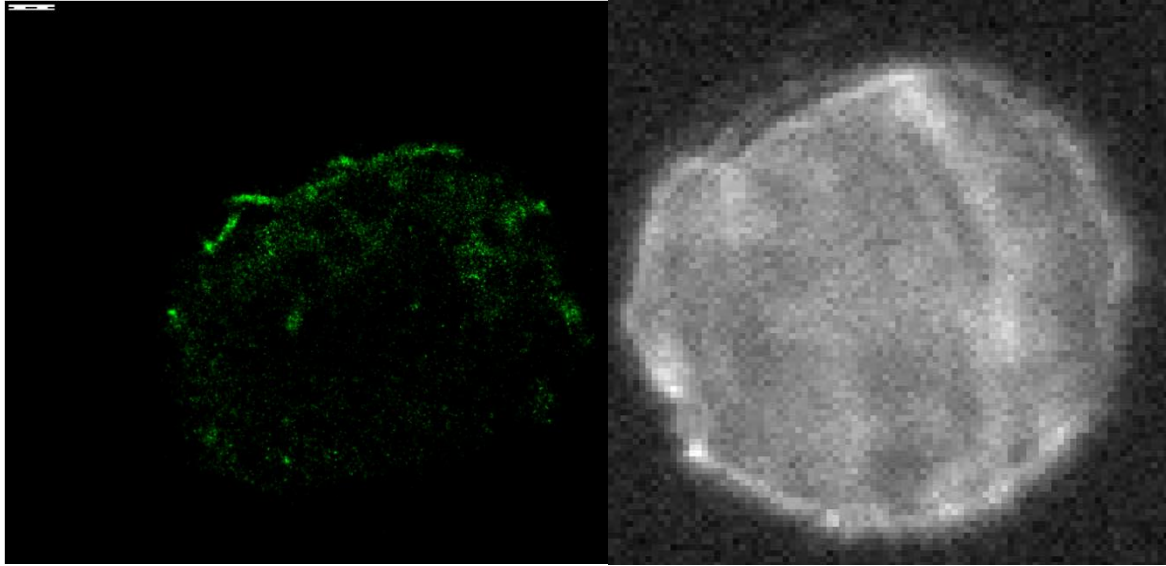


Figure 3.3: A rendered image of Dendra 2-HA in an NIH3T3 cell. A rendered image of Dendra 2-HA in a NIH3T3 cell is shown on the left next to the transmitted light image of the same NIH3T3 cell (right). The scale bar in the left top left corner of the rendered image for Dendra 2-HA in the cell is 500 nm in size.

3.2. Experimental number of photon histograms

The data from each imaged cell was combined from the Einzel-analyzed files to produce Figure 3.4. The histograms of this figure show the number of events versus the number of photons in both the widefield and cross-beam orientations. In both the widefield and cross-beam orientations, the power of the beams at the sample stage was equal. This was done to consider exclusively the effects of laser polarization as opposed to laser power because both parameters affect excitation rates. On the y-axis of the histograms is number of events, while the x-axis is the number of photons.

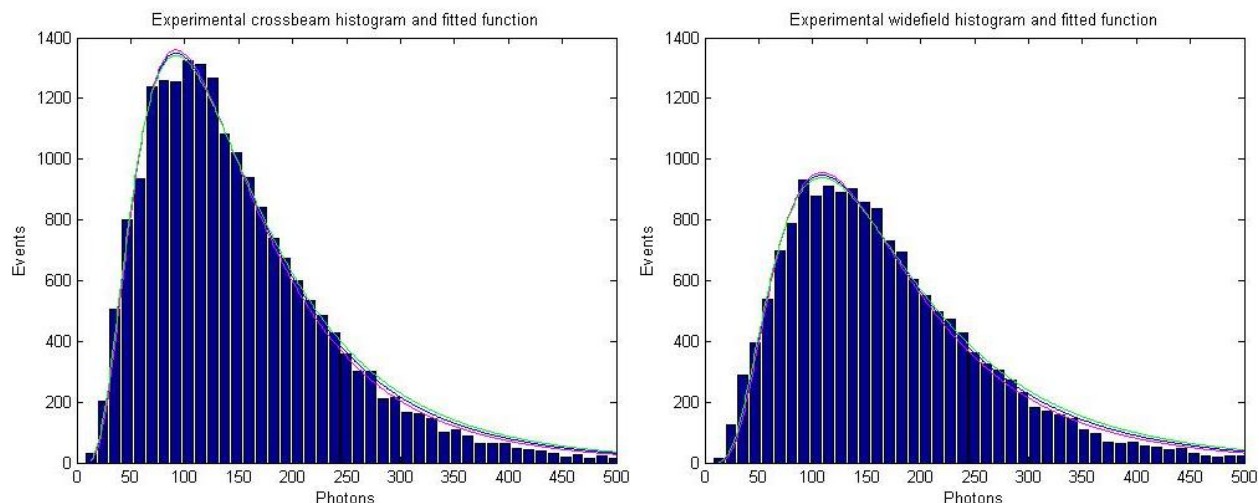


Figure 3.4: Experimental number of photons per localization per frame. Experimental number of photons per localization per frame histograms only show data for those that emitted for three or more consecutive frames. The cross-beam histogram is on the left, while the widefield is on the right. A peak of $93, \pm 0.5$, photons was found under cross-beam illumination, while it was $109, \pm 0.5$, photons for the widefield illumination.

In figure 3.4, an event was qualified as an emission of thirteen or more total photons in a potential localization, but only for those that emitted for three or more frames. Table 3.1 shows the background noise and background noise squared for each analyzed file of the experiment. More trials were run on the widefield than the cross-beam over the same number of cells, which is why the former illumination has fourteen data points, and the latter has twelve. The cross-beam orientation had a background noise squared average value, 4.9, plus or minus a standard deviation, 3.6, photons. The widefield orientation had a background noise squared average value, 6.2, plus or minus a standard deviation, 6.2, photons. In general, the average background noise squared of multiple trials should be greater than or equal to the threshold value to prevent false identification of localizations. If the background noise squared is higher than the threshold, then some background can be falsely identified as localizations.

For these experiments, the threshold was set to a value larger than the average background noise squared plus or minus a standard deviation to prevent this false identification.

Cross-beam		Widefield	
b (background noise)	b²	b (background noise)	b²
1.7	3.1	5.1	26.1
1.7	3.0	2.6	6.7
1.6	2.5	3.2	10.3
2.2	5.0	1.8	3.2
1.8	3.1	2.1	4.3
2.5	6.3	1.7	2.8
3.7	14.0	2.4	5.6
1.3	1.7	1.7	3.0
3.1	9.7	2.0	3.9
2.2	4.7	1.6	2.4
1.5	2.1	2.1	4.6
2.0	4.0	2.7	7.5
		1.8	3.3
		1.7	3.0
Average (b²)	4.9	Average (b²)	6.2
Stdev (b²)	3.6	Stdev (b²)	6.2

Table 3.1. Background noises. Background noises demonstrate a high variation in the widefield orientation in comparison with that of the cross-beam variety. While each illumination imaged the same number of cells, the cross-beam illumination involved two fewer trials, than that of the widefield variety, for imaging five cells.

The emissions that emitted for three or more successive frames are in the histograms of figure 3.4, which has equally spaced bins of width 11.28 photons. The function, $P(x)$, used to fit the experimental histogram was of the form:

$$P(x) = A * \frac{1}{\sqrt{2\pi}xS} e^{\left(\frac{\ln(x)-x_0}{2S^2}\right)^2}$$

The variables A , S and x_0 were used to fit the function to the experimental histogram, and the function itself is that of a lognormal distribution renormalized to fit the data. A

lognormal distribution was used to fit the data because of the skewness of the histogram and

the fact that the excitation rate equation is the result of multiple independent identically distributed variables multiplied together. Initial values were guessed before a Matlab code involving a least-squares fit was used to find the values for parameters within a ninety-five percent confidence interval. From the confidence interval, maximum and minimum values for A , S and x_0 along the interval as well as average values were obtained. These values were used to plot functions with step sizes of one photon.

The full width at half maximum as well as the distance, parallel to the photon axis of the histogram between the maximum value and the maximum photon value where the number of events first drops below the half maximum, were obtained from these functions. Average widths were calculated via the use of the average A , S and x_0 values. Maximum and minimum widths were calculated via the use of maximum and minimum A , S and x_0 values, respectively. Maximum and minimum values of A , S and x_0 were used to calculate uncertainties such that the average width plus or minus an uncertainty value included maximum and minimum widths. Maximum A , S and x_0 correspond to maximum widths, and the converse is true as well. Table 3.1 shows these values for two circularly polarized beams described in section 3.2.1.

Cross-beam fitting 3+ frame histograms				Widefield fitting 3+ frame histograms			
Values	Minimum	Maximum	Average	Values	Minimum	Maximum	Average
A	229000	237000	233000	A	181000	190000	185000
S	0.61	0.63	0.62	S	0.59	0.61	0.60
x_0	4.89	4.92	4.90	x_0	5.03	5.06	5.05

Table 3.2: Experimental A , S and x_0 values. Experimental A , S and x_0 values demonstrate high peak event numbers and lower peak photon numbers for the cross-beam in comparison with the widefield illumination. The S values agree between the widefield and cross-beam orientations. These are the parameters that were used to model the histogram shown in figure 3.4. The maximum and minimum A , S and x_0 values were determined within a ninety-five percent confidence interval.

3.2.1. Both circularly polarized beams

In the case of all localizations that emitted more than thirteen photons, the Gaussian area histogram had less wide full widths at half maximum for the cross-beam illumination, in comparison to the widefield. The angle between the beams was 73 degrees. The excitation rates for the 561 and 532 nm beams were $3.93 \cdot 10^5$ and $2.69 \cdot 10^5 \frac{\text{Watts} \cdot \text{nm} \cdot \text{photons}}{\text{s}}$.

The trend is such that the photon histograms had a smaller full width at half maximum for the cross-beam excitation. This trend was seen in the middle frame(s) for those localizations that emitted for three or more frames in the Gaussian area histograms of figure 3.4. In these graphs, events were restricted only to those localizations that emitted photons for three or more successive frames. Modeling equation parameters for the experimental histograms of figure 3.4 are in table 3.2.

In the case of localizations that emitted photons for three or more frames, the Gaussian area histogram had smaller full widths at half maximum for the cross-beam illumination. The cross-beam illumination over five cells achieved 20225 localizations that emitted for three or more frames. Under the widefield illumination, 16336 localizations were obtained from five cells. A peak of 93 ± 0.5 , photons was found under cross-beam illumination, while it was 109 ± 1 or 109 ± 0.5 , photons for the widefield illumination. The peak number of events for a photon value was found via the use of the lognormal analytical functions used to model the histogram shown in figure 3.4. The experimental average Gaussian area full width at half maximum for the circularly polarized cross-beam and widefield illuminations were 147 ± 3 or 147 ± 4 , and 168 ± 4 or 168 ± 5 photons, respectively. The average width measured

between the maximum event value and the maximum photon value where the event number first drops below half of the maximum was 99, plus 2 or minus 3, and 112 ± 4 photons for the cross-beam and widefield illuminations, respectively.

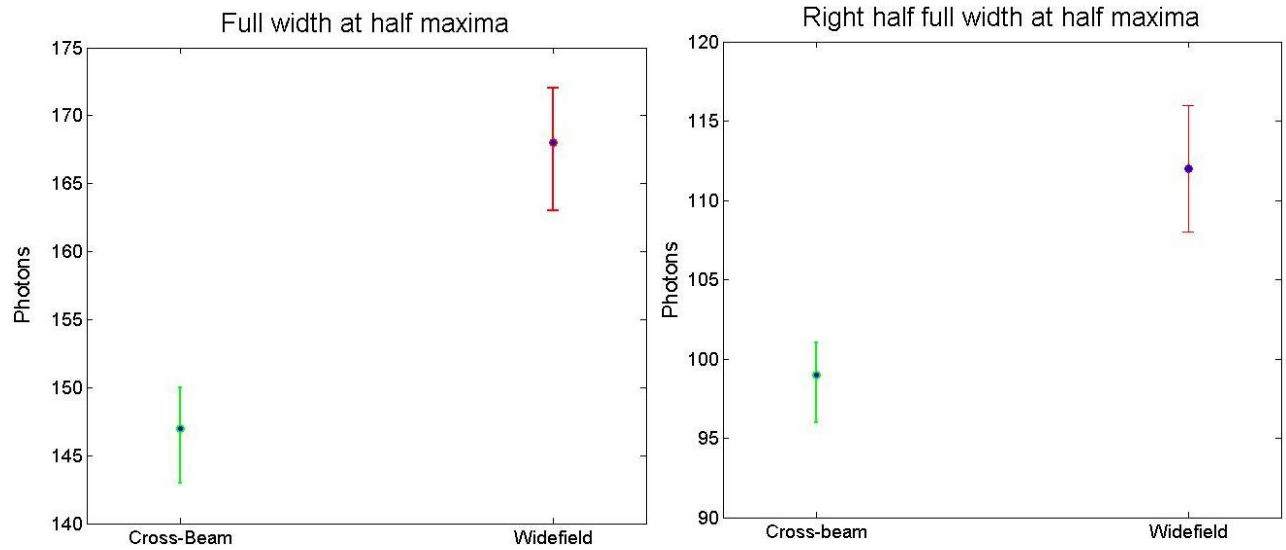


Figure 3.5: Average photon full width at half maxima. The average photon full widths at half maxima with error bars that include the maximum and minimum widths. The maximum and minimum widths were found by a nonlinear fitting of the photon number plots, within a ninety-five percent confidence interval. In the above left plot, the cross-beam has an average of 147, plus 3 or minus 4, photons, while the widefield orientation yielded an average of 168, plus 4 or minus 5, photons. In the above right plot, the cross-beam has an average of 99, plus 2 or minus 3, photons, while the widefield orientation yielded an average of 112 ± 4 photons.

CHAPTER 4

DISCUSSION

4.1. Maximum number of localizations and photon counts

In super-resolution fluorescence localization microscopy (SRFLM), there is a desire to excite all or most fluorophores in a cellular sample with little variation in the number of photons emitted by each fluorophore (Mlodzianoski et al. 2016). In theory, a cross-beam circularly polarized illumination would accomplish this goal more so than a widefield circularly polarized illumination. The comparison was experimentally accomplished via the use of two different excitation wavelengths incident onto a sample with fluorescent proteins on the cell membranes of fixed NIH3T3 cells. Excitation rates were controlled so that only the angle between the beams was varied. Number of photon histograms demonstrate that the cross-beam illumination yielded more localizations and less variation in the number of photons emitted by each fluorophore.

The cross-beam illumination yielded a larger number of localizations that were present for three or more frames because it had more polarizations of light incident onto the sample than that of the widefield variety. This is because a larger number of polarizations of light incident onto a sample increases the probability that more transition dipoles of random orientation will be excited. Evidence of the larger number of localizations can be seen in figure 3.4.

In the widefield illumination, molecules close to the coverslip excite, but also those that are in this same line above and below the plane in focus. The excitation of molecules above and below the plane of focus, in the widefield illumination, is such that the objective is more

likely to pass fluorescence emitted in these regions. This is because the beams are coincident in multiple planes and collinear with the optical axis of the objective. Thus, the molecules above and below the plane of focus are more likely to send photons in a direction such that they would pass through the objective lens. This is seen by the larger average value and greater variation in background noise between the widefield and cross-beam illuminations, as shown in table 3.1.

In the case of the cross-beam excitation, the beams are coincident only in the plane of focus, and nowhere else. Fluorescence where the two beams are not coincident is less likely to pass through the objective because the beams diverge from one another. This lack of coincidence at every place other than the plane of focus, causes the excitations above and below the plane in focus to send photons through the objective lens less often than in the widefield illumination.

4.2. Fluorophore selection based on polarization, number of photons emitted

It is of interest to study polarization effects of the excitation laser as well as molecular orientations within a sample (Gould et al. 2008, Backer et al. 2016). This, in part, is because not detecting certain molecules, due to orientation effects, can cause artifacts in data (Backer et al. 2016). If only a small subset of molecules can be detected, then researchers may not be able to definitively answer important biological questions that require many localizations. Multicolor SRFLM is of interest because researchers can use the tool to study the relationships between two different species of molecule in a sample (Bates et al. 2007, Shroff et al. 2007, Testa et al. 2010, Mlodzianoski et al. 2016). Cross-beam illumination has the potential to help overcome

challenges due to bleed-through and spectral wandering, in multicolor imaging (Mlodzianoski et al. 2016).

Bleed-through comes from uncertainty in the measurement of a spectral ratio, α , where the detection path has a dichroic that transmits or reflects photons based on wavelength. The spectral ratio is calculated by the following equation:

$$\alpha = \frac{I_T}{I_T + I_R}$$

where I_T and I_R are the intensity of the fluorescence in the transmitted and reflected channels, respectively (Gunewardene et al. 2011). The ratio is such that a distribution, and not a discrete number, is obtained for the photons that represent a certain fluorophore. This can cause false colocalization of fluorophores in a sample (Kim et al. 2013). Spectral wandering is such that the spectrum of emission for a fluorophore changes during an imaging session, and can cause false identification of a molecule (Mlodzianoski et al. 2016). Thus, additional further methods of differentiation between fluorophore types, such as brightness, are desirable.

4.3. Simulation results do not agree with those of the experiment

The results of a computer simulation for the experiment, which makes use of principles discussed in section 2.2.10, are shown below. Twenty thousand two hundred twenty-five molecules were simulated in the cross-beam and widefield illuminations to model the number of localizations that emitted for three or more frames in the former illumination. The number of events in the cross-beam simulation peaks at 57 plus 0.5 or minus 1 photons, while the widefield histogram has a peak of 76 ± 1 photons. In the experiment, the number of events peaks at 93 ± 0.5 , for the cross-beam illumination, while it is 109, plus 1 or minus 0.5, photons

for the widefield illumination. The experiment and simulation data are not in agreement with one another for the peak number of photons as mentioned and shown in figure 4.1.

The simulated data were fitted using the least-squares fitting function, $P(x)$, as shown in section 3.2 with maximum, minimum and average full width at half maximum (FWHM) function parameters in table 4.1. Figure 4.1 shows the simulations in bold red with the minimum, maximum and average FWHM functions in pink, green and blue, respectively. Figure 4.2 shows the average FWHM and the right half FWHM values plus or minus the number of photons that encapsulate those of the fitted functions that have the maximum and minimum widths. As is the case with the experimental data, the cross-beam orientation yields smaller photon histograms.

Cross-beam simulation data				Widefield simulation data			
Values	Minimum	Maximum	Average	Values	Minimum	Maximum	Average
A	226000	249000	238000	A	183000	228000	205000
S	0.29	0.32	0.31	S	0.35	0.45	0.4
x0	4.10	4.13	4.12	x0	4.44	4.54	4.49

Table 4.1: A , S and x_0 simulation values with experimental angles and excitation rates. A , S and x_0 simulation values with experimental angles and excitation rates show the same trends as in the experiment, but with a lack of agreement in values for the maximum event and photon numbers. The S values are not in agreement between the cross-beam and widefield illuminations. These are the parameters that were used to model the histogram shown in figure bold red of Figure 4.1. The maximum and minimum A , S and x_0 values were determined within a ninety-five percent confidence interval.

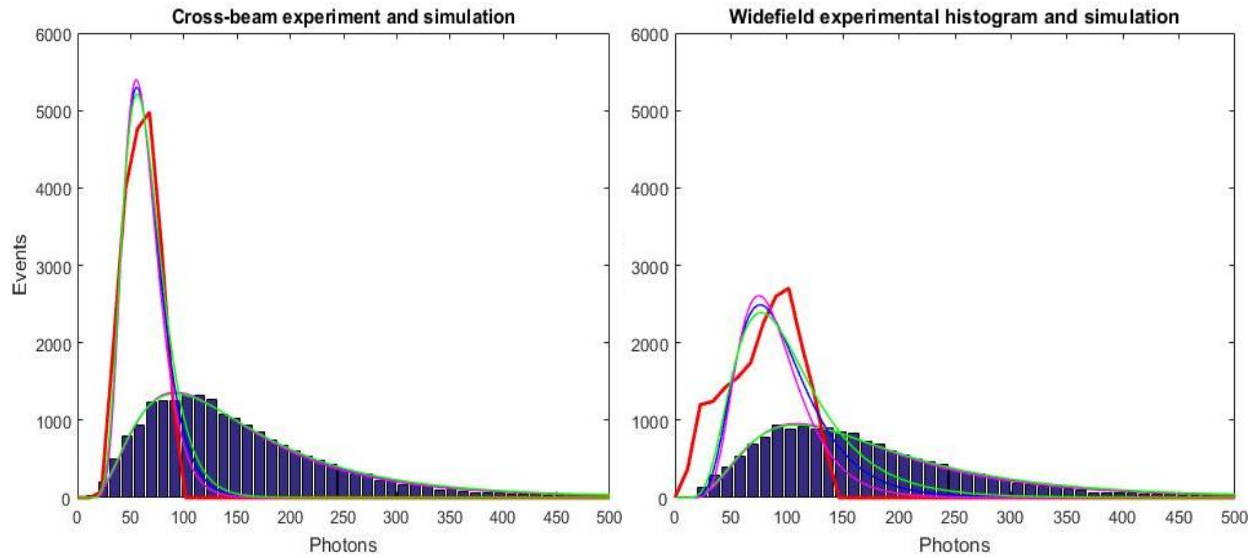


Figure 4.1: Simulation histograms, experimental parameters. The histograms above show simulated data for the number of photons per localization per frame. The cross-beam histogram, at left, has a peak 57 ± 0.5 or minus 1 photons, while the widefield histogram, at right, has a peak of 76 ± 1 photons. The bold red is the simulated data, while the pink, blue and green lines are the minimum, average and maximum fitted functions to the simulation, respectively. The blue histogram boxes show the experimental data with the same parameters.

The simulation average Gaussian area full width at half maximum for the circularly polarized cross-beam and widefield illuminations were 42 ± 3 photons, and 77, plus 10 or minus 9 photons, respectively. The average width measured between the maximum event value and the maximum photon value where the event number first drops below half of the maximum was 25, plus 2 or minus 3, and 47, plus 7 or minus 9, photons for the cross-beam and widefield illuminations, respectively.

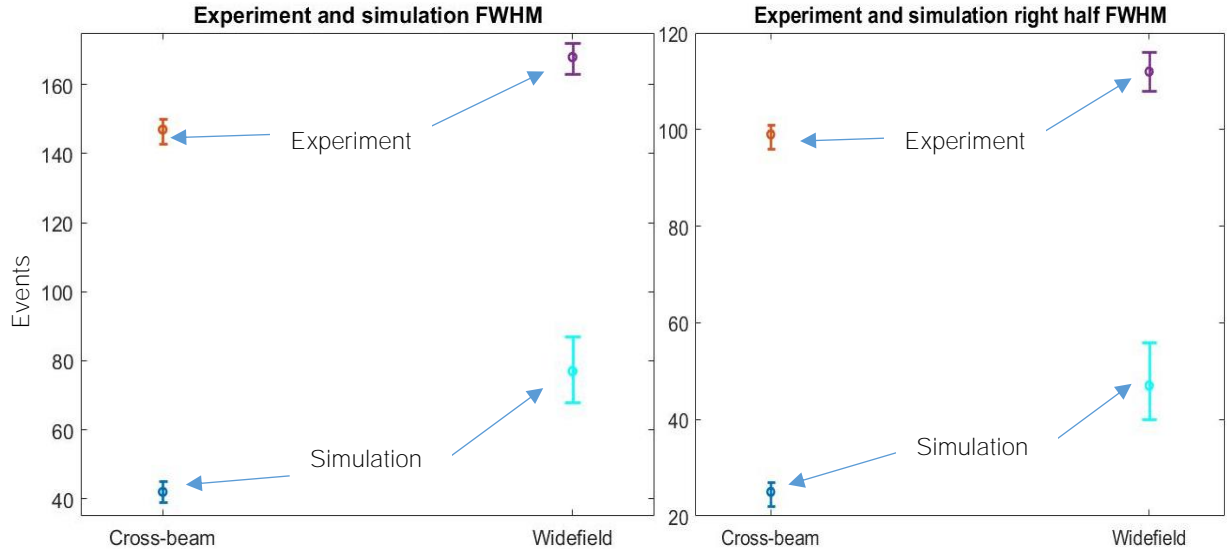


Figure 4.2: Simulation and experiment average full width at half maxima. The above graphs show the experiment and simulation average full widths at half maxima with error bars that include the maximum and minimum widths. The maximum and minimum widths were found by a nonlinear fitting of the photon number histograms, within a ninety-five percent confidence interval. In the above left plot, the cross-beam simulation has an average of 42 ± 3 photons. The widefield orientation, in the same plot, yielded a simulation average of 77 plus 10 or minus 9 photons. In the above right plot, the cross-beam simulation has an average of 25 plus 2 or minus 3 photons. The widefield orientation simulation, in the same plot, yielded an average of 47 plus 7 or minus 9 photons. The experimental FWHMs of figure 3.5 are in these plots for comparison to show that the experiment and simulation are not in agreement with one another.

Although the simulation shows the same trends of decreasing FWHM from widefield to cross-beam illuminations, as well as a decrease in the number of photon peak location, the experimental FWHM is not in agreement with the simulation. Some reasons for the disagreement include blinking, non-uniformities in the beam intensity, incident polarizations and transition dipole orientations. These are discussed in the subsections of this chapter.

4.3.1. Blinking

Blinking makes the simulation used for calculating the brightness of Dendra2 molecules inexact. Blinking molecules involve significant fluctuations in the number of photons emitted per fluorophore per frame going from one to the next. In the blinking process, molecules fluoresce for several milliseconds before not emitting any light and repeating until the molecule permanently bleaches (Dickson et al. 1997).

Blinking causes the number of photon histogram to widen going from the simulation to the experiment because the former makes use of the model shown in figure 4.3. In this model, there is no fluorescence until the fluorophore starts emitting. It does not start fluorescing until sometime in the second frame, then emits steadily for the duration of all the frames until sometime during the second to last frame. Sometime during the second to last frame the fluorophore photobleaches, so that it does not emit light in the last frame.

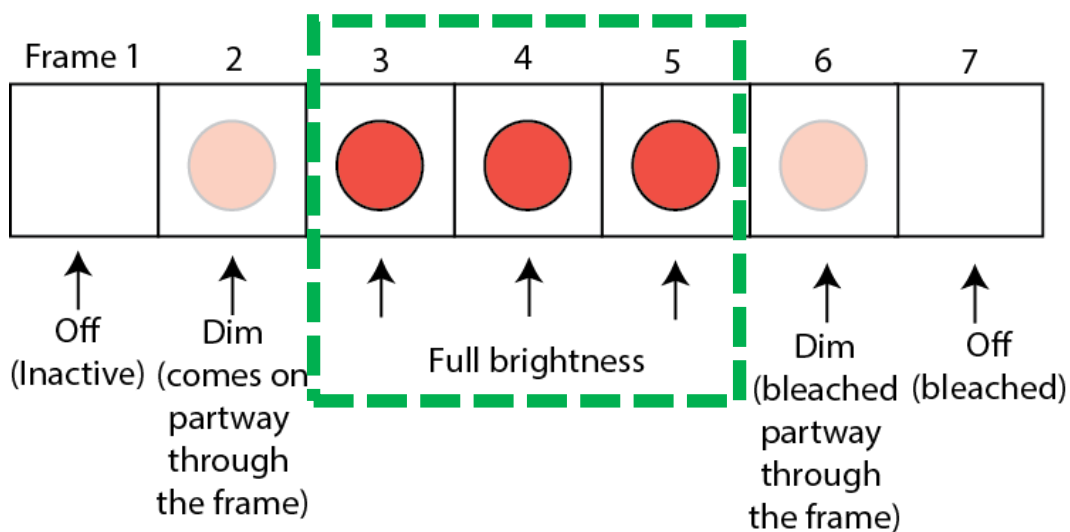


Figure 4.3: Simulation model. The model used as a guide for writing the simulation and deciding which experimental frames to use of the localizations that emitted for three or more frames. Middle frame number of photon information was used because at some time during the second and second to last frames when the fluorophore emits light, the fluorophore begins and ceases to emit photons, respectively. This model does not consider effects due to blinking.

Experimental blinking is shown in figure 4.4 for 694 localizations in a cell. Some variations in the number of photons emitted per localization per frame involve hundreds of photons larger than the FWHM values measured in the experiment. This is a significant reason for the disagreement between the experimental and simulation FWHM values.

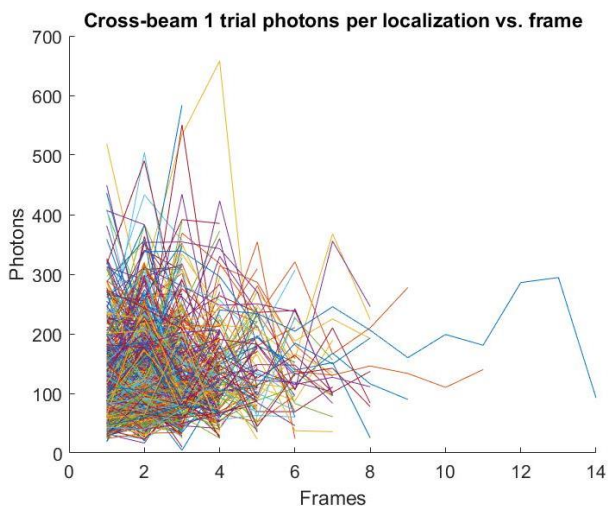


Figure 4.4: Experimental blinking for 694 localizations. Experimental blinking for 694 localizations show wide variability in the number of photons per localization per frame in the cross-beam orientation. Molecules emit light and fluctuate in the amount of light they emit per frame until they emit no longer after the last frame.

Factors that affect blinking include intrinsic properties of the fluorophore as well as the local environment, especially in the sample pH (Bagshaw et al. 2006, Hoogenboom et al. 2006, Yeow et al. 2006, Haupts et al. 1998, Hess et al. 2004). In a fixed sample, it might be possible to make the pH such that the blinking disappears and not affect live cellular functions. The samples used in the experiments involved a pH of 7 because they were imaged in UV-bleached phosphate buffer solution.

Experimentally, it would be important to mitigate effects due to blinking that will aid in decreasing the variation in brightness. In the simulation, it would be helpful to include blinking

in the computer code to model what was seen in the experiments. The simulation model would include parameters that would involve molecules fluorescing with some variation, between one frame and the next, to model the trend of figure 4.4.

4.3.2. Non-uniformities in the beam intensity

Experimentally, the 561 and 532 nm beams had 10.4 and 11.4 micron one over e-squared radii, respectively. These beams were used to image an approximately circular area with a 4.5-micron radius. The beams were aligned so that their centers were in the middle of the imaging area.

However, the experimental beam profile is not perfectly Gaussian. As shown in figure 3.2, the experimental beams are slightly elliptical. This is different from the simulation, which involves a perfect Gaussian, so can also partially cause differences between the simulation and experiment.

4.3.3. Laser incident polarizations

In the experiment, the laser polarizations were such that they were not completely circular. A linear polarizer was used to test the efficacy of the quarter wave plate in observing whether the beams were circularly polarized. It was placed after the quarter wave plate in the beam path, with a power meter on the sample stage. The linear polarizer was rotated, and the power of the beam observed to calculate the minimum power divided by the maximum for a quarter wave plate setting. A one hundred percent ratio between the minimum and maximum power means that the beam is circularly polarized, which is experimentally very difficult to achieve. Thus, an eighty percent ratio was achieved, with the quarter wave plate set to an

angle that maximized the ratio. The quarter wave plate was then used experimentally to compare between the cross-beam and widefield circularly polarized illuminations' effects on the photon number histograms. The simulation made use of one hundred percent circularly polarized light, which would allow for all polarizations to be accessed equally in the plane of the laser beams. Thus, this difference between eighty percent and one hundred percent circular polarization partially accounts for a difference in the experimental and simulated FWHMs.

4.3.4. Transition dipole orientations

In the simulation, transition dipole orientations were set to be random. Experimentally, the dipoles orientations were not measured in the detection path. Thus, the dipole orientations may have been predominantly in one direction as opposed to another. This is another possible reason for differences between the simulated and experimental data. A future experiment could make use of polarization selection in the detection path to separate and observe the emission polarizations in a sample, and could be guided by simulation results shown in figures 4.5 and 4.6.

4.4. Future directions

The experimental results and simulation give some understanding of what can be done to further decrease the widths of the photon histograms. The experimental powers of each beam have not been optimized for yielding a high number of localizations with a small FWHM, as shown in the comparison between the experimental and simulation histograms. Equal excitation rates as well as a ninety-degree angle between the beams can yield greater decreases in the FWHM, as is shown in figure 4.6.

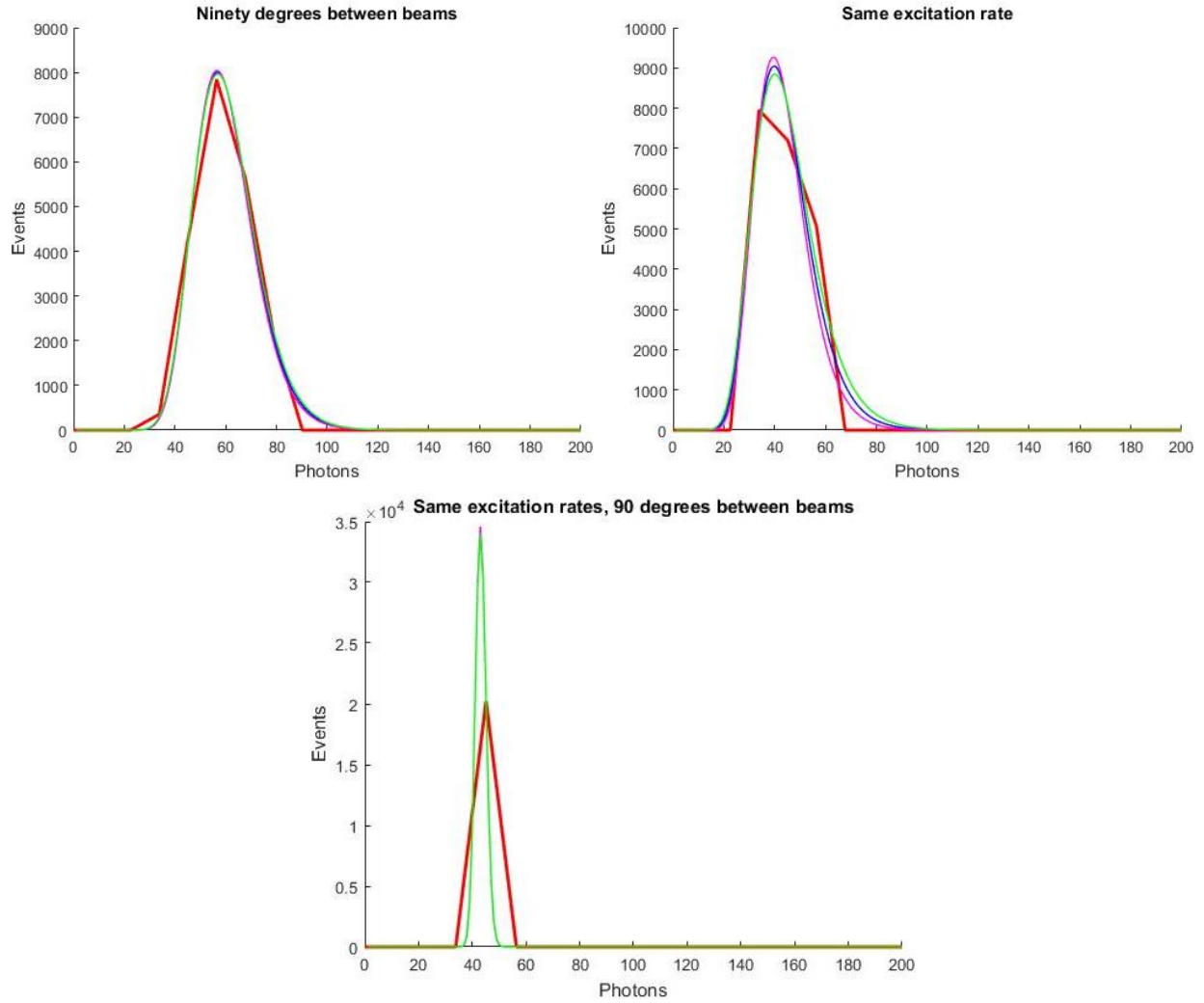


Figure 4.5: Simulation histograms, ideal parameters. The above simulation histograms make use of the parameters used in the experiment except for those mentioned in the title of each histogram. The above left histogram features 90 degrees between the beams with everything else the same as in the experiment, while the above right has the same excitation rate of $3.93 \cdot 10^5 \frac{\text{Watts} \cdot \text{nm} \cdot \text{photons}}{\text{s}}$ for both beams. The bottom middle histogram involves both $3.93 \cdot 10^5 \frac{\text{Watts} \cdot \text{nm} \cdot \text{photons}}{\text{s}}$ for both excitation beams with a ninety-degree angle between them. The number of particles imaged is the same for each simulation, and the full width at half maximum decreases from the histogram at left to the one at right. Peaks from the analytical functions are 41 for the top left histogram, 58 for the top right histogram and 44 for the bottom middle histogram, all plus or minus 0.5 photons. The maximum number of photons is 10000 on the y-axis of the above right graph, 9000 for the above left and 35000 for the bottom middle.

With a ninety-degree angle between the beams and the same excitation rates as in the experiment, the peak number of photons is 41 ± 0.5 . For the simulation that involves the same excitation rate of $3.93 \cdot 10^5 \frac{\text{Watts} \cdot \text{nm} \cdot \text{photons}}{\text{s}}$, but with an experimental value of 73 degrees between the beams, the peak value for the number of photons is 58 ± 0.5 . With a ninety-degree angle and $3.93 \cdot 10^5 \frac{\text{Watts} \cdot \text{nm} \cdot \text{photons}}{\text{s}}$ excitation rates, the simulation yields a peak number of 44 ± 0.5 photons.

The simulation average Gaussian area full width at half maximum for ninety degrees between the beams, equal excitation rates of $3.93 \cdot 10^5 \frac{\text{Watts} \cdot \text{nm} \cdot \text{photons}}{\text{s}}$ and both features together are 28, plus 1 or minus 0.5, 26 ± 2 , and 6 ± 0.5 , photons, respectively. The average width measured between the maximum event value and the maximum photon value, where the event number first drops below half of the maximum was 15, plus 1 or minus 0.5, 15, plus 1 or minus 2, and 3 ± 0.5 , photons for ninety degrees between the beams, equal excitation rates of $3.93 \cdot 10^5 \frac{\text{Watts} \cdot \text{nm} \cdot \text{photons}}{\text{s}}$ and both features, respectively.

Furthermore, two circularly polarized beams are not as efficient as one circularly polarized beam with another beam that is linearly polarized in a direction that is perpendicular to the plane of the circularly polarized beam. One linearly polarized beam with one circularly polarized beam can allow for less bias away from the linear polarizations that are perpendicular, or close to perpendicular to one another, in the two beams. The powers could be optimized for this orientation to decrease the photon histogram width and increase the number of localizations in a sample.

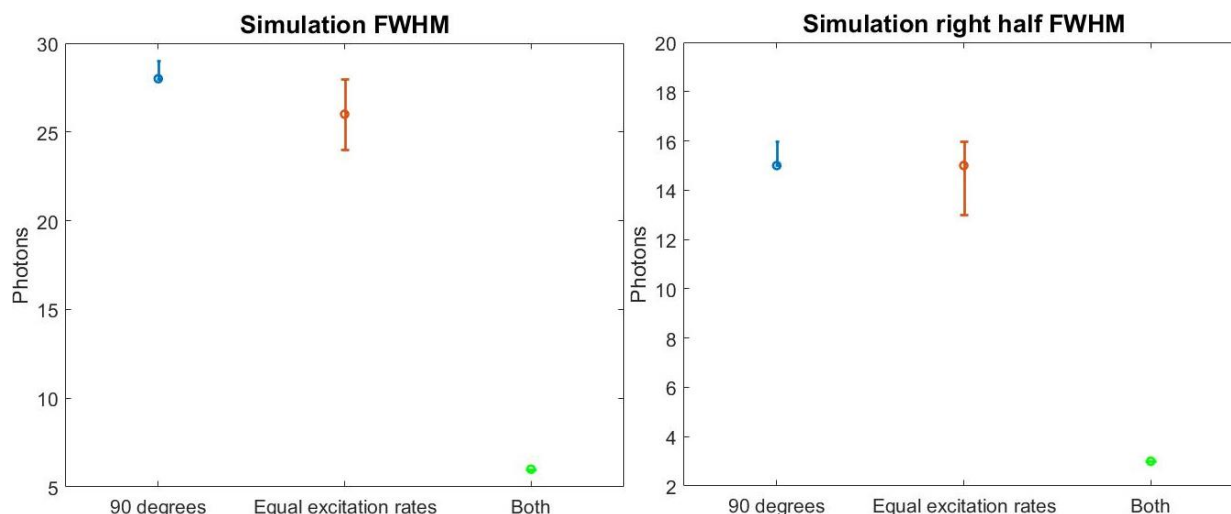


Figure 4.6: Simulated average FWHM, ideal parameters. The simulated average FWHM plus and minus the maximum and minimum, respectively, for the histograms of figure 4.5 show that both 90 degrees and equal excitation rates yield the smallest full width at half maximum. For ninety degrees between the beams with everything else the same as in the experiment, the FWHM and right half FWHM are 28 and 15 plus 1 or minus 0.5 photons. For equal excitation rates with everything else the same as in the experiment, the FWHM and right half FWHM are 26 ± 2 photons and 15 plus 1 or minus 2 photons, respectively. For equal ninety degrees between the beams and equal excitation rates with everything else the same as in the experiment, the FWHM and right half FWHM are 6 and 3 ± 0.5 , photons, respectively.

Cross-beam illumination decreases the number of photon histogram distribution width.

The illumination can be used in conjunction with conventional multicolor imaging to differentiate between fluorescent molecular species. The spectral ratio in combination with the molecule brightness could improve the precision of molecular identification.

Real-time analysis could be used to further decrease the histogram width to allow for changing the power in between trials of imaging a cell. Due to the analysis aspect of this work, one cannot know whether a cell's fluorophores have emitted a particular number of photons

until after the experiment has been analyzed. A real-time analysis computer program, with a capability to produce number of photon histograms, almost instantaneously, could allow for decreasing the widths of said histograms by adjusting the excitation laser intensities.

A project that expands on polarization studies, and aids in decreasing the width of the photon number histograms, may involve spatial modulation such that a circularly polarized excitation beam would circularly rotate in the back aperture of the objective lens. This rotation would selectively excite different orientations of transition dipoles at different times. One could make use of two-dimensional galvanometer mirrors to spatially move the beams in a circle on the back focal plane (Johnson et. al 2014). The modulation could be tuned to maximize the fluorescence of a sample via the use of fluorescent beads as well as a back-reflection intensity detector (Johnson et al 2014). Modulations on the same timescale as the millisecond order time frames over which fluorescence happens in dyes and proteins as well as the frame rates (Johnson et al. 2014). A schematic of the alignment is shown in figure 4.7.

For membrane proteins, a TIRF alignment with rotation might allow for a higher number of localizations to be achieved with more selective brightness. This is because a TIRF alignment with rotation would cause less background and be able to excite more different dipole orientations of molecules than widefield and tilted alignments. This is because the evanescent field that results from a TIRF alignment penetrates only ~100 nm above the coverslip, close to which the lipids, dyes, or proteins are imaged. The widefield and tilted alignments, in comparison with the TIRF alignment, penetrate more deeply because the beam goes up and through the sample. As a result of the beams going up and through the sample in widefield and tilted illuminations, molecules above and below a plane of interest are likely to emit light. This

causes increased background, which impedes identification and localization of the molecules in the plane of interest, which ultimately degrades the spatial resolution.

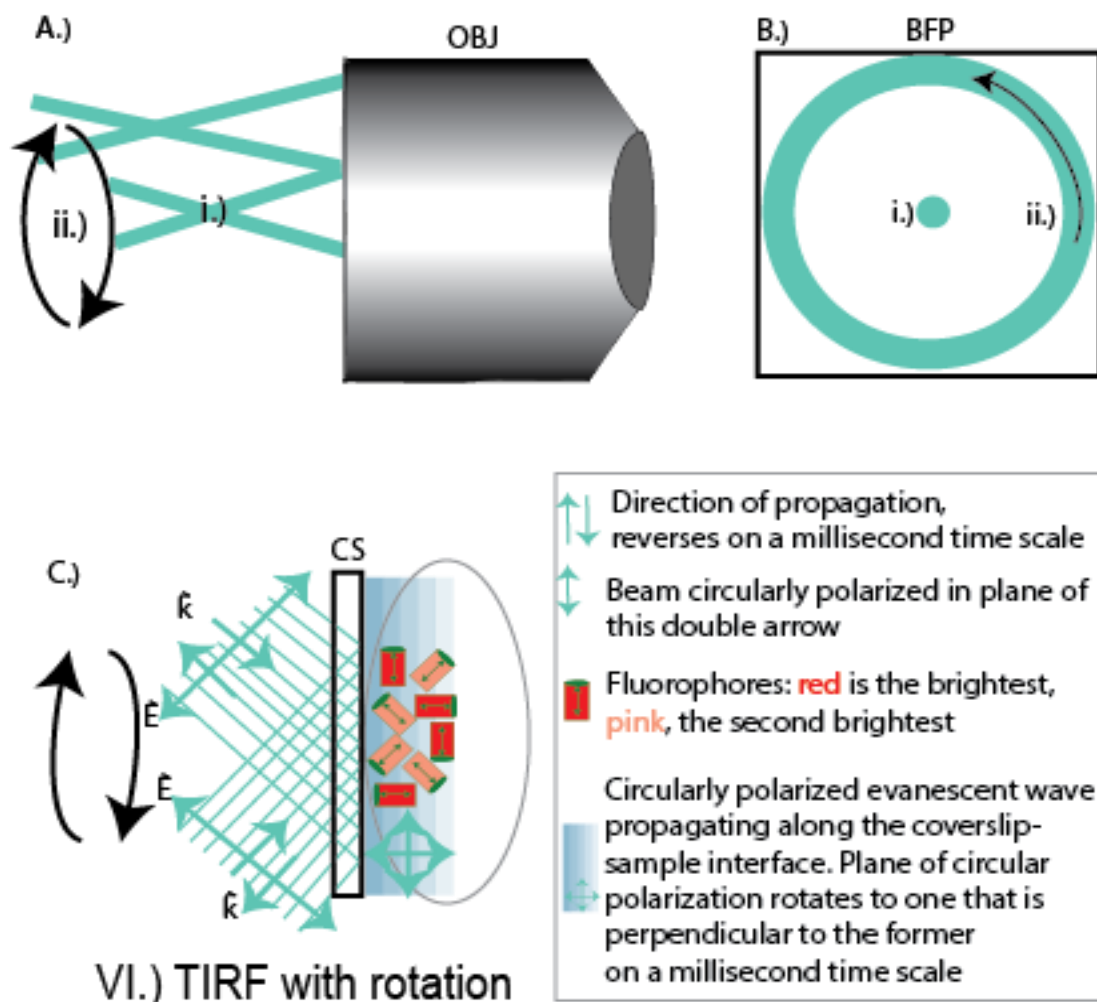


Figure 4.7: TIRF with rotation diagram. VI.) TIRF with rotation involves the excitation laser beam moving in a circle on the back focal plane (BFP). A side view of the BFP is in A.), with a frontal view in B.), and on the side of the coverslip (CS) in C.). In i.) is the widefield orientation. The beam goes straight through the center of the back focal plane, and is focused at a point, one focal length distance away from the objective lens. ii.) The beam moves in a circle on the back focal plane (BFP), so that the beam is focused at the same point as in the widefield orientation, but with the evanescent wave from the TIRF alignment exciting fluorophores that are perpendicular to the widefield orientation beam's electric field.

The rotation of circularly polarized light in the back aperture would allow for a larger number of dipole orientations to be accessed. Thus, additional orientations of molecules along with lower background could be obtained via the use of the TIRF illumination with rotation

alignment in comparison to one of the widefield or tilted variety. In this way, imaging membrane proteins or dyes would be improved if a TIRF alignment with a rotating beam were used to image them through the use of a two-dimensional galvanometer mirror.

4.4.1. Multicolor imaging

The cross-beam illumination could be applied and used well in multicolor imaging. One could use the method to image fluorophores that have distinct emission peaks to improve identification of these fluorophores. For example, actin, PIP2 and hemagglutinin have been of interest among other groups of proteins, lipids and ions due to their role in how the flu virus infects (Gunewardene et al. 2011, Gudheti et al. 2013, Mlodzianoski et al. 2016). The way that these molecular species move about and colocalize on the cell membrane is important for understanding how the flu virus enters into and assembles within host cells. It is critical to optimize correct identification and minimize the mis-identification of fluorophores to allow localization data to be correctly interpreted in the context of influenza infection and other biological functions. Thus, the cross-beam illumination could be used to image a few of these species together for the sake of understanding more about how to prevent the spread of the flu virus.

In another application, there is present the desire to observe interactions between lipids and proteins in the cell membrane via the use of SRFLM (Curthoys et al. 2015). The cell membrane is made up of two opposing monolayers comprised of proteins, lipids and other small molecules. An example of a cell membrane is in figure 4.7, modeled after the lipid raft theory. The model involves lipids that can self-organize and form discrete patches in the cell

called rafts that are made up of sphingolipids, cholesterol, as well as transmembrane and glycosylphosphatidylinositol-anchored (GPI-anchored) proteins. Proteins can either be raft-associated or non-raft associated depending on their affinity to the self-organizing lipids (Curthoys et al. 2015).

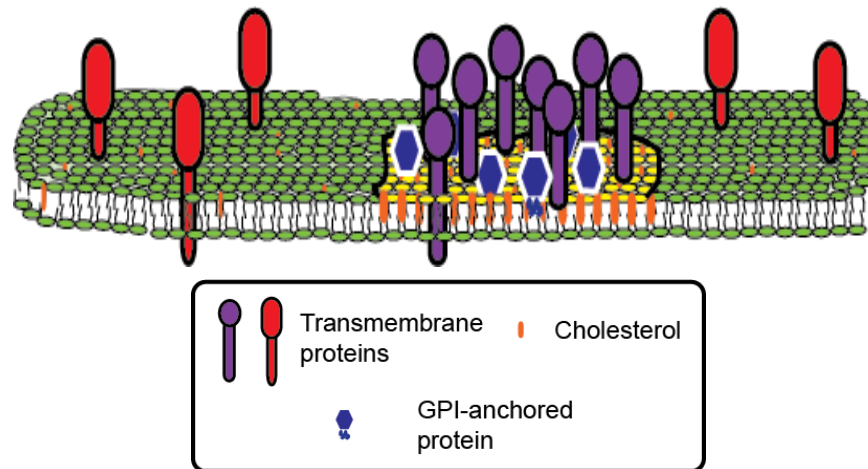


Figure 4.8: Lipid raft model. The lipid raft model shows sphingolipid and cholesterol patches populated with proteins that have an affinity for said patches. Protein species can be raft associated or non-raft associated (Curthoys et al. 2015).

The lipid raft is one of a few that scientists use to understand and interpret what they observe in a cell membrane (Curthoys et al. 2015). A cross-beam experiment with a multicolor module may be used with a lipid dye and Dendra2-HA to obtain information about how they colocalize and move with respect to one another. Information about colocalization and diffusion could be used to see how well the lipid raft, among other models, describe what is observed. The experimental set-up for this experiment is in figure 4.8.

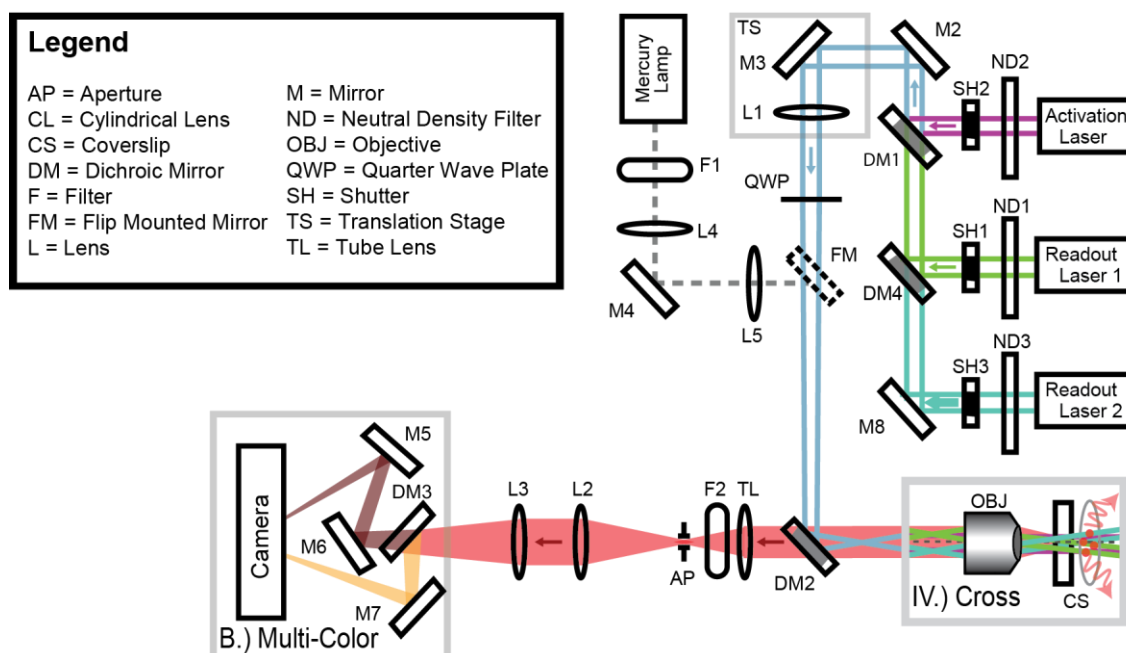


Figure 4.9: A multicolor imaging detection path with cross-beam orientation. A multicolor imaging detection path with the cross-beam orientation can lead to better identification of molecules. This set-up is the same as in 2.1, but with a multicolor detection module, and only the cross-beam orientation shown. In the multicolor module, dichroic mirror DM3 splits up fluorescence based on wavelength of light to separate emission spectra from one another. The separated emissions then reflect off mirrors onto two distinct places on the camera chip, so that they can be imaged in separate channels. The path lengths between the reflection off, and transmission through, the dichroic to the camera, are equal so that the same plane is imaged in both channels. The fluorophores would need to be of a wavelength such that they could be excited by the two lasers of a similar wavelength.

4.4.2. Single color multispecies imaging

If the beam polarization and power could be fine-tuned to have immense control over the molecule brightness, then it may be possible to use the illumination to differentiate between molecules that have similar excitation and emission spectra. Two fluorophores of interest could be imaged individually using the cross-beam orientation in separate cellular samples. After analyzing the number histograms to find the peak number of photons per fluorophore as well as the width of the single histogram, one could image both fluorophores

together with the same cross-beam orientation. The data collected from the single-color experiments, particularly the location of the average photon peak, as well as the width of said peak, could be used to see where the different molecules are present and how they are fixed or moving about with respect to each other. This experiment could work especially well with a lipid dye and protein that excite and emit at similar wavelengths because the former emits many more photons than the latter, upon excitation.

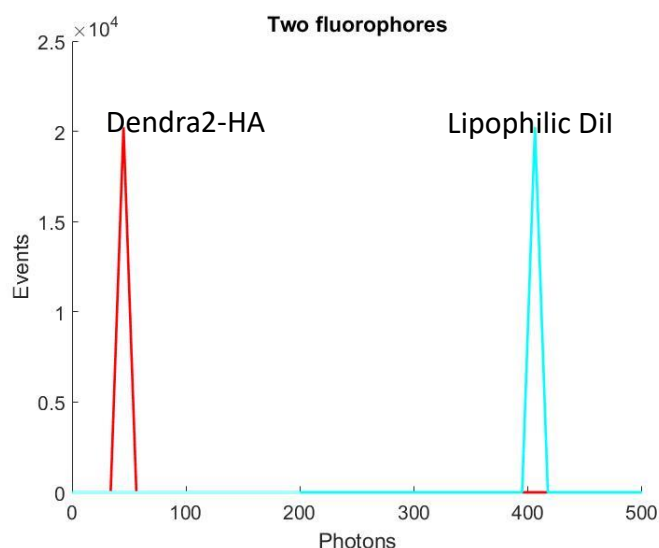


Figure 4.10: Simulation of Dendra2 and lipophilic DiI number of photon histograms. Simulation of Dendra2 and lipophilic DiI number of photon histograms. Lipophilic DiI has an extinction coefficient greater than $1.25 \times 10^5 \text{ cm}^{-1} \text{ M}^{-1}$ (Molecular Probes Inc. 2008). With a cross-sectional area that has an extinction coefficient so many times the size of Dendra2, ninety degrees between the 532 and 561 nm lasers and each beam causes an excitation rate of $3.93 \times 10^5 \frac{\text{Watts} \cdot \text{nm} \cdot \text{photons}}{\text{s}}$, maximum, one gets the result shown in the figure (Molecular Probes Inc. 2008).

Excitation and emission spectra for Dendra2 and lipophilic DiI are distinct, but also somewhat overlapping. Because of the differences in absorption spectrum, the excitation rates from both the 561 and 532 nm laser would be different for at least one of the fluorophores. Lipid DiI has a peak excitation of 549 nm and a peak emission of 565 nm (Molecular Probes Inc.

2008). The emission spectra for lipophilic DiI is shown in figure 4.10 for lipophilic dyes in a phospholipid bilayer membrane.

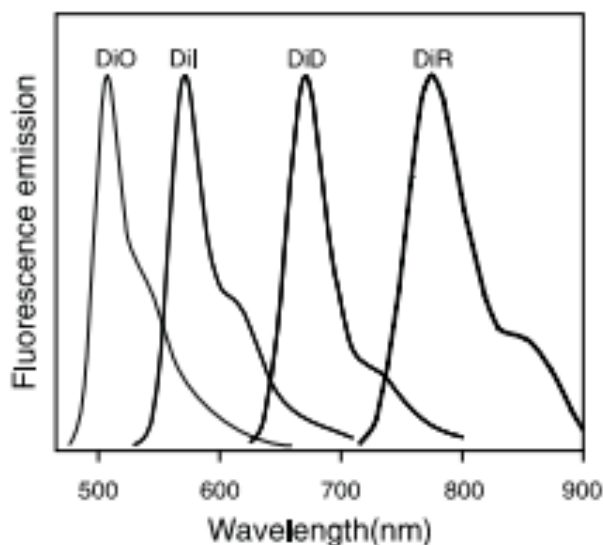


Figure 4.11: Normalized fluorescence emission spectra of DiO, DiI, DiD, and DiR bound to phospholipid bilayer membranes. Normalized fluorescence emission spectra of DiO, DiI, DiD, and DiR bound to phospholipid bilayer membranes (Molecular Probes Inc. 2008).

If at least one of multiple fluorophores imaged had equal excitation rates from the 561 and 532 nm lasers, it would be helpful in terms of distinguishing between them based on width and location of the number histogram peak. Furthermore, a sample with more than two fluorophores excited by the same lasers, in a similar manner, might be more distinguishable among the species in the sample.

Future work in multicolor imaging would improve both because of a decreasing variation in the number of photons emitted by fluorophores in a sample and increase in the number of localizations (Mlodzianoski et al. 2016). Cross-beam imaging decreases the variation in brightness and increases the number of localizations. This is because the illumination type

increases the probability of exciting more fluorophores, and can help to excite differently oriented fluorophores more equally. Thus, the method can mitigate issues of multicolor imaging such as bleed-through and spectral wandering so that one can achieve a deeper understanding of the system they study.

4.4.3. Mitigating emitted photon variation due to blinking

Problems related to blinking must be solved for the sake of optimal use of cross-beam illumination. Some ways to mitigate the blinking of Dendra2 include raising the pH and lowering the excitation rate by decreasing the power of the laser at the sample stage (Pennacchietti et al. unpublished), which will also require longer acquisition time per frame. Raising the pH or lowering the excitation rate by decreasing the laser power at the sample stage would be tested, independently, before combining these two features for the sake of decreasing the FWHM of the photon number histogram.

Besides getting rid of the blinking by changing the pH or excitation power, another way to mitigate effects due to blinking involves changing the camera frame rate. A high frame rate and short acquisition time could allow for emissions to be either in an on or off state as viewed by the camera. This could greatly decrease the variation in the emission of photons, even to the point that there is only a state of being on or off, as viewed by the camera. This would be challenging to implement, given the wide range of emissions from the fluorophores that blink. Those that emit upwards of hundreds of photons may be the only ones that can be seen with such a high frame rate. With a high frame rate to mitigate effects due to blinking, one might

not be able to visualize clusters very well, given that only the brightest of fluorophores will be seen by the camera.

A low frame rate and high acquisition time may allow for more averaging over the number of photons emitted by fluorophores. To average over the number of photons emitted by fluorophores could involve histograms showing the number of photons per localization rather than the number of photons per localization per frame. This type of averaging could be used to show whether the widefield or cross-beam orientation makes fluorophores emit with less variation in brightness. A combination of increasing the pH as well as decreasing the excitation power and frame rate, could yield the best molecular identification based on brightness. This combination could serve well in molecular identification studies of the future.

REFERENCES

- Backer, A. S., Lee, M. Y., & Moerner, W. E. (2016). Enhanced DNA imaging using super-resolution microscopy and simultaneous single-molecule orientation measurements. *Optica*, 3(6), 659–666.
- Baddeley, D., Cannell, M. B., & Soeller, C. (2010). Visualization of localization microscopy data. *Microscopy and Microanalysis*, 16(01), 64–72. <http://doi.org/10.1017/S143192760999122X>.
- Bagshaw, C. R., & Cherny, D. (2006). Blinking fluorophores: what do they tell us about protein dynamics? *Biochemical Society Transactions*, 34(5), 979–982.
- Bates, M., Huang, B., Dempsey, G. T., Zhuang, X., & Dempsey, T. (2007). Multicolor Super-Resolution Imaging with Photo-Switchable Probes Fluorescent. *Science*, 317(5845), 1749–1753. <http://doi.org/10.1126/science.1146598.Multicolor>.
- Betzig, E., Patterson, G. H., Sougrat, R., Lindwasser, O. W., Olenych, S., Bonifacino, J. S., Davidson, M.W., Lippincott-Schwartz, J., Hess, H. F. (2006). Imaging intracellular fluorescent proteins at nanometer resolution. *Science (New York, N.Y.)*, 313(5793), 1642–5. <http://doi.org/10.1126/science.1127344>.
- Born, M. & Wolf, E. (1997). “Principles of optics: electromagnetic theory of propagation, interference and diffraction of light”. New York, Cambridge University Press.
- Bossi, M., Fölling, J., Belov, V. N., Boyarskiy, V. P., Medda, R., Egner, A., Eggeling, C., Schoenle, A., Hell, S. W. (2008). Multicolor far-field fluorescence nanoscopy through isolated detection of distinct molecular species. *Nano Letters*, 8(8), 2463–2468. <http://doi.org/10.1021/nl801471d>.
- Curthoys, N. M., Parent, M., Mlodzianoski, M., Nelson, A. J., Lilieholm, J., Butler, M. B., Valles, M.M., Hess, S. T. (2015). *Dances with Membranes: Breakthroughs from Super-resolution Imaging. Current Topics in Membranes* (Vol. 75). Elsevier Ltd. <http://doi.org/10.1016/bs.ctm.2015.03.008>
- Curthoys, N. M., Mlodzianoski, M. J., Kim, D., & Hess, S. T. (2013). Simultaneous multicolor imaging of biological structures with fluorescence photoactivation localization microscopy. *Journal of Visualized Experiments: JoVE*, (82), e50680. <http://doi.org/10.3791/50680>.
- Dickson, R. M., Cubitt, A. B., Tsien, R. Y., & Moerner, W. E. (1997). On / off blinking and switching behaviour of single molecules of green fluorescent protein. *Nature*, 388(July), 355–358.

- Gould, T. J., Gunewardene, M. S., Gudheti, M. V., Vladislav, V., Yin, S., Gosse, J. A., & Hess, S. T. (2008). NIH Public Access, 5(12), 1027–1030. <http://doi.org/10.1038/nmeth.1271>.Nanoscale.
- Gould, T., Hess, S., & Bewersdorf, J. (2012). Optical nanoscopy: from acquisition to analysis. *Annual Review of Biomedical Engineering*, (2), 231–254. <http://doi.org/10.1146/annurev-bioeng-071811-150025>.Optical.
- Gould, T. J., Verkusha, V. V., & Hess, S. T. (2009). NIH Public Access. *Nature Protocols*, 4(3), 291–308. <http://doi.org/10.1038/nprot.2008.246>.Imaging.
- Gudheti, M. V., Curthoys, N. M., Gould, T. J., Kim, D., Gunewardene, M. S., Gabor, K. A., Gosse, J. A., Kim, C. H., Zimmerberg, J., Hess, S. T. (2013). Actin mediates the nanoscale membrane organization of the clustered membrane protein influenza hemagglutinin. *Biophysical Journal*, 104(10), 2182–2192.
- Gunewardene, M. S., Subach, F. V., Gould, T. J., Penoncello, G. P., Gudheti, M. V., Verkhusha, V. V., & Hess, S. T. (2011). Superresolution imaging of multiple fluorescent proteins with highly overlapping emission spectra in living cells. *Biophysical Journal*, 101(6), 1522–1528. <http://doi.org/10.1016/j.bpj.2011.07.049>.
- Gurskaya N.G., Verkhusha V.V., Shcheglov A.S., Staroverov D.B., Chepurnykh T.V., Fradkov A.F., Lukyanov S., Lukyanov K.A. Engineering of a monomeric green-to-red photoactivatable fluorescent protein induced by blue light. *Nature Biotechnology*. 2006; 24 (4):461-5.
- Haupts, U., Maiti, S., Schwille, P., & Webb, W. W. (1998). Dynamics of fluorescence fluctuations in green fluorescent. *Proceedings of the National Academy of Sciences of the United States of America*, 95(November), 13573–13578.
- Hell, S. (2007). Far-Field Optical Nanoscopy. *Science*, 2(May), 1153–1158. <http://doi.org/10.1126/science.1137395>.
- Hess, S. T., Heikal, A. A., & Webb, W. W. (2004). Fluorescence Photoconversion Kinetics in Novel Green Fluorescent Protein pH Sensors. *Journal of Physical Chemistry B*, 10138–10148.
- Hess, S. T., Girirajan, T. P. K. & Mason, M. D. (2006). Ultra-high resolution imaging by fluorescence photoactivation localization microscopy. *Biophysical Journal*, 91, 4258-4272.
- Hess, S. T., Gould, T. J., Gudheti, M. V., Maas, S. a, Mills, K. D., & Zimmerberg, J. (2007). Dynamic clustered distribution of hemagglutinin resolved at 40 nm in living cell membranes discriminates between raft theories. *Proceedings of the National Academy of Sciences of the United States of America*, 104(44), 17370–17375.

- Hoogenboom, J. P., den Otter, W. K., & Offerhaus, H. L. (2006). Accurate and unbiased estimation of power-law exponents from single-emitter blinking data. *The Journal of Chemical Physics*, 125(204713), 1–13. <http://doi.org/10.1063/1.2387165>
- Huang, B., Wang, W., Bates, M., & Zhuang, X. (2007). Three-Dimensional Super-Resolution Imaging by Stochastic Optical Reconstruction Microscopy. *Science*, 319, 810-813. <http://science.sciencemag.org.prxy4.ursus.maine.edu/content/sci/319/5864/810.full.pdf>.
- Huang, F., Hartwich, T. M. P., Rivera-Molina, F. E., Lin, Y., Duim, W. C., Long, J. J., Uchil, P. D., Myers, J. R., Baird, M. A., Mothes, W., Davidson, M. W., Toomre, D., Bewersdorf, J. (2013). Video-rate nanoscopy using sCMOS camera-specific single-molecule localization algorithms. *Nature Methods*, 10(7), 653–8. <http://doi.org/10.1038/nmeth.2488>.
- Johnson, D. S., Toledo-crow, R., Mattheyses, A. L., & Simon, S. M. (2014). Polarization-Controlled TIRFM with Focal Drift and Spatial Field Intensity Correction. *Biophysical Journal*, 106(5), 1008–1019. <http://doi.org/10.1016/j.bpj.2013.12.043>.
- Juette, M. F., Gould, T. J., Lessard, M. D., Mlodzianoski, M. J., Nagpure, B. S., Bennett, B. T., Hess, S.T., Bewersdorf, J. (2008). Three-dimensional sub-100 nm resolution fluorescence microscopy of thick samples. *Nature Methods*, 5(6), 527–9. <http://doi.org/10.1038/nmeth.1211>.
- Kim, D., Curthoys, N. M., Parent, M. T., & Hess, S. T. (2013). Bleed-through correction for rendering and correlation analysis in Multi-Colour Localization Microscopy. *Journal of Optics*, 15(9), 1–30. <http://doi.org/10.1088/2040-8978/15/9/094011.Bleed-through>.
- Lakowicz, J. R. (2006). “Principles of fluorescence spectroscopy”. New York, Springer.
- Manley, S., Gillette, J. M., Patterson, G. H., Shroff, H., Hess, H. F., Betzig, E., & Lippincott-Schwartz, J. (2008). High-density mapping of single-molecule trajectories with photoactivated localization microscopy. *Nature Methods*, 5(2), 155–157. <http://doi.org/10.1038/nmeth.1176>.
- Mlodzianoski, M. J., Schreiner, J. M., Callahan, S. P., Smolková, K., Dlasková, A., Santorová, J., ... Bewersdorf, J. (2011). Sample drift correction in 3D fluorescence photoactivation localization microscopy. *Optics Express*, 19(16), 15009–19. Retrieved from <http://www.ncbi.nlm.nih.gov/pubmed/21934862>.
- Mlodzianoski, M. J., Valles, M. M., & Hess, S. T. (2016). Super Resolution Fluorescence Localization Microscopy. *Encyclopedia of Cell Biology*. *Encyclopedia of Cell Biology*. Elsevier. <http://doi.org/10.1016/B978-0-12-394447-4.20090-4>.
- Molecular Probes Inc. (2008). Lipophilic Tracers—Dil, DiO, DiD, DiA, and DiR. *Invitrogen*, 1–6.

- Mortensen, K. I., Churchman, L. S., Spudich, J. A., & Flyvbjerg, H. (2010). HHS Public Access. *Nature Methods*, 7(5), 377–381. <http://doi.org/10.1016/bs.mcb.2015.01.016>. Observing
- The Nobel Prize in Chemistry 2014 - Press Release. *Nobelprize.org*. Nobel Media AB 2014. http://www.nobelprize.org/nobel_prizes/chemistry/laureates/2014/press.html.
- Pennacchietti, F., Nelson, A. J., & Hess, S. T. Unpublished. The Photophysics of Dendra2 and its Role in Localization Microscopy.
- Rust, M. J., Bates, M. & Zhuang, X. W. 2006. Sub-diffraction-limit imaging by stochastic optical reconstruction microscopy (STORM). *Nature Methods*, 3, 793-795.
- Shim, S.-H., Xia, C., Zhong, G., Babcock, H. P., Vaughan, J. C., Huang, B., Wang, X., Cheng, X., Gui-Qiang, B., Zhuang, X. (2012). Super-resolution fluorescence imaging of organelles in live cells with photoswitchable membrane probes. *Proceedings of the National Academy of Sciences*, 109(35), 13978–13983. <http://doi.org/10.1073/pnas.1201882109>.
- Shroff, H., Galbraith, C. G., Galbraith, J. A., White, H., Gillette, J., Olenych, S., Davidson, M.W., Betzig, E. (2007). Dual-color superresolution imaging of genetically. *Proceedings of the National Academy of Sciences of the United States of America*, 104(51), 20308–20313. <http://doi.org/10.1073/pnas.0710517105>.
- Testa, I., Wurm, C. A., Medda, R., Rothermel, E., Von Middendorf, C., Fölling, J., Jakobs, S., Schoenle, A., Hell, S. W., Eggeling, C. (2010). Multicolor fluorescence nanoscopy in fixed and living cells by exciting conventional fluorophores with a single wavelength. *Biophysical Journal*, 99(8), 2686–2694. <http://doi.org/10.1016/j.bpj.2010.08.012>.
- Thompson, R. E., Larson, D. R., & Webb, W. W. (2002). Precise Nanometer Localization Analysis for Individual Fluorescent Probes. *Biophysical Society*, 82(May 2002), 2775–2783.
- Yeow, E. K. L., Melnikov, S. M., Bell, T. D. M., Schryver, F. C. De, & Hofkens, J. (2006). Characterizing the Fluorescence Intermittency and Photobleaching Kinetics of Dye Molecules Immobilized on a Glass Surface. *Journal of Physical Chemistry A*, 110(5), 1726–1734.

APPENDIX

SUPPORTING INFORMATION

1. Average intensity Calculator MATLAB computer program

The MATLAB code for calculating the average intensity is given below, and was written by Dr. Andrew J. Nelson. The code produces the following outputs:

1/e² radius (microns)
Average intensity (kW/cm²)
Power (mW)

The outputs above come from the following inputs:

pwr: laser power in milliwatts
q: pixel size in micrometers
des_int: desired average intensity of laser
1 tiff file showing the beam profile as shown in chapter 3

Andrew Nelson and Matthew Valles wrote this code

```
clear all
clc

global xpix ypix wbox;

pwr = 28; %laser power in mw;
q = 0.132; %pixel size in um
des_int = 5890; % W/cm^2 of desired average intensity

%%%%%%%%%%%%%%%%%%%%%%%%%%%%%%%%%%%%%%%%%%%%%%%%%%%%%%%%%%%%%%%%%%%%%%%%
%%%%%%%%%%%%%%%%%%%%%%%%%%%%%%%%%%%%%%%%%%%%%%%%%%%%%%%%%%%%%%%%%%%%%%%%
% Use GUI to load the image file
%%%%%%%%%%%%%%%%%%%%%%%%%%%%%%%%%%%%%%%%%%%%%%%%%%%%%%%%%%%%%%%%%%%%%%%%
%%%%%%%%%%%%%%%%%%%%%%%%%%%%%%%%%%%%%%%%%%%%%%%%%%%%%%%%%%%%%%%%%%%%%%%%

cur = pwd; %Find the current directory
% if isappdata(0, 'Last_Directory')
```

```

% last_dir = getappdata(0, 'Last_Directory');
% if last_dir ~= 0
%     if exist(last_dir,'dir')
%         cd(last_dir);
%     end
% end
% end
[fname,pname] = uigetfile({'*.tif','*.tiff Files'},'Select tiff file containing beam profile:');
if fname~=0 %load the appropriate mat file if valid
    img_file = [pname,fname];
else
    return
end
if pname ~=0
    if exist(pname,'dir')
        setappdata(0, 'Last_Directory', pname);
    end
end
cd(cur); %Reset active directory

%%%%%%%%%%%%%%%%%%%%%%%%%%%%%%%%%%%%%%%%%%%%%%%%%%%%%%%%%%%%%%%%%%%%%%%%%%%%%%
%%%%%%%%%%%%%%%%%%%%%%%%%%%%%%%%%%%%%%%%%%%%%%%%%%%%%%%%%%%%%%%%%%%%%%%%%%%%%%
% Use GUI to select the region to be analyzed
%%%%%%%%%%%%%%%%%%%%%%%%%%%%%%%%%%%%%%%%%%%%%%%%%%%%%%%%%%%%%%%%%%%%%%%%%%%%%%
%%%%%%%%%%%%%%%%%%%%%%%%%%%%%%%%%%%%%%%%%%%%%%%%%%%%%%%%%%%%%%%%%%%%%%%%%%%%%%

i1=imread(img_file,1);
h = figure('WindowStyle','modal','NumberTitle','off','Name',...
    'Select Region For Laser Profile:',...
    'Pointer','cross','Units','Normalized','OuterPosition',[0 0 1 1]);
set(h,'Units','Pixels');
imagesc(i1,'HitTest','off');
axis image
colormap gray
drawnow
try %gets coordinates of user selected ROI
    waitforbuttonpress
catch
    return
end
p1 = get(gca,'CurrentPoint');
rbbox;
p2 = get(gca,'CurrentPoint');

```

```

close(h);
pause(.1); %makes sure figure closes

p1 = double(uint16(round(p1(1,1:2)))+1); %Image indexes start at 1 but CurrentPoint starts at 0,
p2 = double(uint16(round(p2(1,1:2)))+1); %offset by 1 is to resolve this

if(p1(1) < p2(1))
    x1 = p1(1);
    x2 = p2(1);
else
    x2 = p1(1);
    x1 = p2(1);
end
if(p1(2) < p2(2))
    y1 = p1(2);
    y2 = p2(2);
else
    y2 = p1(2);
    y1 = p2(2);
end

grab=double(i1(y1:y2,x1:x2));

[sizey,size_x] = size(grab);

% Make the chosen area to be square
if (size_x < size_y)
    grab = grab(1:size_x, 1:size_x);
    size_img = size_x;
else
    grab = grab(1:size_y, 1:size_y);
    size_img = size_y;
end

% Make the image size odd
if mod(size_img,2) == 0
    grab = grab(1:size_img-1, 1:size_img-1);
    size_img = size_img-1;
end

wbox = size_img;
rbox = round((size_img-1)*0.5);
[xpix,ypix] = meshgrid(-rbox:rbox,-rbox:rbox);

```

```

[row col] = find(grab == max(grab(:)),1,'first');
[row1, col1] = find(round(grab) == round(max(grab(:))*exp(-1/2)));
disx = row1 - row;
disy = col1 - col;

dist = (disx.^2 + disy.^2).^0.5;
sigma = max(dist);

% Find the center of mass for initial guess in fit
xm_sum = 0;
ym_sum = 0;
m_sum = 0;

for i = 1:wbox
    for j = 1:wbox
        xind = floor(i);
        yind = floor(j);
        intens = grab(yind, xind);
        xm_sum = xm_sum + xind*intens;
        ym_sum = ym_sum + yind*intens;
        m_sum = m_sum + intens;
    end
end

x_cm = xm_sum/m_sum;
y_cm = ym_sum/m_sum;

xc_box = (1+size_img)*0.5;
yc_box = (1+size_img)*0.5;

xguess = x_cm - xc_box;
yguess = y_cm - yc_box;

xymerge(wbox*wbox) = 0;
zmerge(wbox*wbox) = 0;

for i=1:wbox
    for j=1:wbox
        k = (i-1)*wbox+j;
        xymerge(k) = 0;
        zmerge(k) = grab(i,j);
    end
end

```



```

beta0 = [xguess, yguess, max(max(grab)), 2*sigma, min(min(grab))];
[betafit,resid,J,COVB,mse] = nlinfit(xymerge,zmerge,@gaussian_merge3,beta0);
ci = nlparci(betafit,resid,'covar',COVB); %calculate error estimates on parameters
ci_err=(ci(:,2)-ci(:,1))/2;

yf = betafit(2) + yc_box;
xf = betafit(1) + xc_box;
a0 = betafit(3);
r0 = abs(betafit(4));
off = betafit(5);

failed=0; %flag for failed localization
if(a0 < 0)
    failed=1;
end
if(xf > wbox || xf < 1 || yf > wbox || yf < 0)
    failed=1;
end

r0_um = r0*q; %convert r0 from pixel to um
r0_cm = r0_um*1e-4; %convert r0 from um to cm
pwr = pwr/1000; %convert power from mW to W

I0 = pwr/((1/2)*pi*r0_cm^2);

r0
r0_um
% I0

des_pow = des_int * pi * (r0_um*10^-4)^2;

disp(['for an average intensity of ', num2str(des_int/1000), 'kW/cm^2 you should use ',
num2str(des_pow*1000), 'mW of laser'])

```

2. Pixel size calculator MATLAB computer program

This code produces the pixel size in microns via the use of a scale image. An example of a scale image is shown in Figure 3.3. Dr. Andrew J. Nelson wrote this computer code:

```

%%%%%%%%%%%%%%%%%%%%%%%%%%%%%%%%%%%%%%%%%%%%%%%%%%%%%%%%%%%%%%%%%%%%%%%%
%%%%%%%%%%%%%%%%%%%%%%%%%%%%%%%%%%%%%%%%%%%%%%%%%%%%%%%%%%%%%%%%%%%%%%%%
% A script to estimate the micron per pixel value given a scale image

```

```

%
% This program accepts a tiff image of a scale image. The image should be
% oriented so that the scale bars are lying horizontal, and separated by a
% vertical distance, relative to this screen. (i.e. should look like a
% ladder)
%
% You will be asked questions relating to your optical setup. The code is
% already setup to handle both the Hamamtsu sCMOS and the Andor iXon
% cameras available in the lab.
%
% You are required to put in an expected pixel value based off of a manual
% measurement. This tells the program to look in a window around the
% expected value, and helps reduce errors in the analysis.
%
% One the image is loaded and the questions are answered, you are asked to
% select a region in the image to analyze. This is done by zooming into the
% image allowing you to select the appropriate region for analysis. Once
% zoomed in, press 'enter' and click 5 points (4 points of a rectangle and
% the 5th to enclose the region in a polygon) to indicate which area you
% want analyzed
%
% In my experience choosing a narrow region with many bars works best.
%
% This program can still analyze out of focus images.
%
% AJN 5/4/14
%%%%%%%%%%%%%%%%%%%%%%%%%%%%%%%%%%%%%%%%%%%%%%%%%%%%%%%%%%%%%%%%%%%%%%%%%%%%%%
%%%%%%%%%%%%%%%%%%%%%%%%%%%%%%%%%%%%%%%%%%%%%%%%%%%%%%%%%%%%%%%%%%%%%%%%%%%%%%
clear all
close all
clc

%% Load the data file into the workspace
[fname1, fpath1] = uigetfile('*.tif','Choose a file to analyze');
uncropped = double(imread((strcat(fpath1,fname1))));
addpath(pwd);
cd(fpath1);
clims = [min(uncropped(:)), max(uncropped(:))];
%% plot the data
f1 = figure;
screen_size = get(0, 'ScreenSize');
set(f1, 'Position', [0 0 screen_size(3) screen_size(4) ] );
h = imshow(uncropped,clims);
axis equal

```

```

scmos = input('Did you use the sCMOS camera for this experiment? y or n ','s');
if strcmp(scmos,'y') || strcmp(scmos,'Y')
    real_pix = 6.4; % real pixel size in microns
else
    real_pix = 16;
end
obj_mag = input('What magnification objective did you use? ');
tel_str = input('What was the approximate magnification of your telescope? ');
% expected_pix = input('What is your expected pixel size in nm? ');
totalmag = tel_str*obj_mag;
expect_pix = real_pix/totalmag;
scale_sep = 10; % scale separation size in microns


% get current axes
p=gca;
hold on
% maskx = zeros(size(
%defines the number of vertices one will be selecting
num_of_vert = 5;
result = input('Press enter once zoomed in');
%% creat a polygon that encloses the roi
for w = 1:num_of_vert
    clearvars points;
    % selects point clicked in plot
    disp('Choose an area to measure');
    waitforbuttonpress;
    points = get(p,'currentpoint');

    % assigns selected points to array
    poly_vert(w,1) = points(1,1);
    poly_vert(w,2) = points(1,2);

    % draws polygon on plot in red
    plot(poly_vert(:,1),poly_vert(:,2),'r');

end
saveas(f1, strcat(fpath1, fname1(1:numel(fname1)-4), '_figure.fig'), 'fig');
hold off
% poly_vert = ([6.041099636 11.3361058; 6.364811368 11.54877688 ; 7.731176006
10.07513568; 7.482746072 9.911397765; 6.044863726 11.32481353]);

cropped =

```

```

uncropped(min(poly_vert(:,2)):max(poly_vert(:,2)),min(poly_vert(:,1)):max(poly_vert(:,1)));

% fst_crop = gpuArray(cropped);
C1_gpu = xcorr2(cropped);
C1 = gather(C1_gpu);
[yind,xind] = find(C1==max(C1(:)));
plot(1:numel(C1(:,1)),C1(:,xind));
title('Autocorrelation along the vertical axis');
ylabel('Correlation a.u. ');
xlabel('Displacement in pixels');
center = (numel(C1(:,1))+1)/2;
non_rot = horzcat((1:numel(C1(:,1))))',C1(:,xind));

% Define each point as a vector and split the distribution in half about
% the center
non_rot1 = non_rot(1:center,:);
% non_rot2 = fliplr(non_rot(center:numel(C1(:,1))),:).';
% non_rot2(:,1) = non_rot1(:,1);

% rotate the vectors by the angle created with the origin and maximum central point
theta1 = atan(non_rot1(end,2)/non_rot1(end,1));
rot1 = zeros(numel(non_rot1(:,1)),2);
rot2 = zeros(numel(non_rot1(:,1)),2);
rot1(:,1) = cos(-theta1).*non_rot1(:,1) - sin(-theta1).*non_rot1(:,2);
rot1(:,2) = sin(-theta1).*non_rot1(:,1) + cos(-theta1).*non_rot1(:,2);
figure
plot(rot1(:,1),rot1(:,2))
title('Rotated autocorrelation curve');

% Find the peaks in the distribution
peaks1 = findpeaks(rot1(:,2));
index1 = ismember(rot1(:,2),peaks1);

%% This section is redundant considering the symmetry of the data
%% do it again for the second half of the distribution
% theta2 = atan(non_rot1(end,2)/non_rot1(end,1));
%
% rot2(:,1) = cos(-theta2).*non_rot2(:,1) - sin(-theta2).*non_rot2(:,2);
% rot2(:,2) = sin(-theta2).*non_rot2(:,1) + cos(-theta2).*non_rot2(:,2);
% plot(rot2(:,1),rot2(:,2))
% peaks2 = findpeaks(rot2(:,2));
% index2 = ismember(rot2(:,2),peaks2);
% % program's guesses in pixels

```

```

guess1 = center-(cos(theta1).*rot1(index1,1)-sin(theta1).*rot1(index1,2));
% guess2 = -center+cos(theta2).*rot2(index2,1)-sin(theta2).*rot2(index2,2);

% all guesses combined in um
allguess = scale_sep./guess1;
% second_guess = scale_sep./guess1(index2);

[val ind_gue] = min(abs(allguess*1000-expect_pix));

if abs(allguess(ind_gue)*1000-expect_pix)/expect_pix > 0.2;
    ind_gue = find(allguess > 0.8*expect_pix & allguess<1.2*expect_pix );
end
end_guess = allguess(ind_gue);
per_err = abs(end_guess-expect_pix)/expect_pix;
actual_mag = real_pix/end_guess;
disp(['Measured a pixel size of ', num2str(end_guess), 'um which is in ',
num2str(per_err*100),'% error of the calculated value']);
disp(['Calculated pixel size: ', num2str(expect_pix)]);
disp(['Expected Magnification: ', num2str(totalmag),'X']);
disp(['Measured Magnification: ', num2str(actual_mag),'X']);
%attempts to rotate autocorrelation to find

% clearvars -except uncropped cropped poly_vert fname1 fpath1 C1
%
%
% save(strcat(fname1(1:numel(fname1)-4),'_analyzed.mat'));
%
% % answer = input('Load a rendered image of total cell? (y/n)','s');
% % if answer == 'y'
% %     [fname2, fpath2] = uigetfile('*.tif','Choose a rendered image');
% %     image1 = imread(strcat(fpath2,fname2));
% %     mask = roipoly(image1,poly_vert(:,1),poly_vert(:,2));
% end

```

3. Calculate trajectories matlab computer program

This computer program was produced by Andrew Nelson. It takes an Einzel-analyzed file and calculates trajectories for localizations in a data set, based on a minimum distance between two localizations in successive frames. If the two localizations are within that distance from one another, then they are considered part of the same trajectory. The code and its scripts are in A.3. The outputs of this program are two .mat files that are used with the Einzel code for further analysis via the use of the program in A.4.

```

%%%%%%%%%%%%%%%%%%%%%%%%%%%%%%%%%%%%%%%%%%%%%%%%%%%%%%%%%%%%%%%%%%%%%%%%
%%%%%%%%%%%%%%%%%%%%%%%%%%%%%%%%%%%%%%%%%%%%%%%%%%%%%%%%%%%%%%%%%%%%%%%%
% This is a master batch file for testing trajectories.
% The script will perform the trajectory analysis at various dmax values
% then offer a plot to show the response of diffusion coefficient and
% number of trajectories found vs. dmax
% weight_ave gives out the average diffusion coefficient of a particular
% dmax value
% created 5/1/14 AJN
% This codes was built off of previously used codes

clear all
clc

dmax=0.3; %max distance (in um) in next frame to be considered as a pair
dfactor=2; %if next-nearest is within dmax*dfactor in the next frame, don't count as a pair
dfactor2=2; %if any within dmax*dfactor2 in the same frame, don't count as a pair
microns_per_pixel=0.132; %camera pixel size
exp_time = 0.01; % frame exposure time in seconds
savename = 'mitocells.mat';

dirname='J:\121316\Analysis\Cell 2 Analysis\'; %choose where you want the outputs to be
saved

%% Pair Identification
%dirname='C:\Users\Sam\Desktop\2Color_LiveCell\Analysis\05-14-
2010\Analysis\CytoD_Dendra2-HA_PAmCherry-Actin\tolerances052410\';
cd(dirname);
files=dir(fullfile(dirname,'*_t13.mat'));
N_files=size(files);
mol_type=1;
for dmax = .070 % this for loop chooses various sizes of dmax to analyze
for cont1=1:N_files(1);

    this_file=files(cont1).name;
    this_file=this_file(1:end-4);
    matfile=strcat(dirname,this_file,'.mat');
%    index=find(this_file=='_tol');
    save_name=strcat(dirname,'_',this_file,'_',num2str(dmax*1000),'nm_connect.mat');

    %data_all=[index_c index_n frame_c frame_n xc yc NN_dx NN_dy NN_dist_c NN_dist_n
    NNN_dist_n a0_c a0_n]
    [q,dist_data,xf_all,yf_all,framenum_all,total_molecules,nrat,green_sum,red_sum]=next_fram
e_dist_func_TG1_2color3AJN(matfile,microns_per_pixel,dmax,dfactor,dfactor2,mol_type);

```

```

%load(matfile,'xf_all','yf_all','framenum_all','a0_all','total_molecules','nrat','green_sum','red_s
um');
%stop
save(save_name,'q','xf_all','yf_all','nrat','red_sum','green_sum','dist_data','microns_per_pixel
','dmax','dfactor','dfactor2');
end
end

%% Trajectory creator
files_con=dir('*_connect.mat');
N_files_con=size(files_con);

for i=1:N_files_con(1);

    this_file=files_con(i).name;
    this_file=this_file(1:end-4);
    matfile=strcat(dirname,this_file,'.mat');
%    index=find(this_file=='_');
    save_name=strcat(matfile(1:end-4),'_traj.mat');

    trajectories_func;
end

%% Trajectory analysis
File_Info=dir('*_traj.mat');
nfiles=length(File_Info);
Ds_all = zeros(N_files(1,1),round(5/0.05));
num_o_traj = zeros(N_files(1,1),round(5-0.05));
for j=1:nfiles
    clear ds_all_ave num_con dmax

    mat_name=File_Info(j).name;
    [ds_all_ave, num_con, dmax]=trajectory_analysis_func(dirname,mat_name,exp_time);
    if exist('dmax_ind','var')
        index = find(ismember(dmax_ind,dmax));
        if 1 isempty(index)
            iddqd = find(Ds_all(:,index)==0,1);
            Ds_all(iddqd,index) = ds_all_ave;
            num_o_traj(iddqd,index) = num_con;
        else
            dmax_ind = vertcat(dmax_ind,dmax);
            Ds_all(1,numel(dmax_ind)) = ds_all_ave;
            num_o_traj(1,numel(dmax_ind)) = num_con;
        end
    end
end

```

```

else
    dmax_ind = dmax;
    Ds_all(1,1) = ds_all_ave;
    num_o_traj(1,1) = num_con;
end
end

%% creates weighted averages of diffusion coefficients based on number of molecules
measured in each file
for lk = 1:numel(dmax_ind)
    weight_ave(lk) = sum(num_o_traj(:,lk). *Ds_all(:,lk))/(sum(num_o_traj(:,lk)));
    tot_num(lk) = sum(num_o_traj(:,lk));
    err_diff(lk) = std(Ds_all(:,lk));
end

%% Representing the data
figure
subplot(2,1,1)
errorbar(dmax_ind,weight_ave,err_diff,'b');
title('Diffusion Coefficient vs. dmax');
xlabel('dmax in um');
ylabel('Diffusion Coefficient in um^2/s');

subplot(2,1,2)
plot(dmax_ind,tot_num,'b');
title('Total Number of Trajectories vs. dmax');
xlabel('dmax in um');
ylabel('Number of trajectories found');

%% Makes an estimation of the diffusion coefficient based on total number of trajectories
found
INdex = logical(1-isnan(weight_ave));
diffuse_guess = sum(weight_ave(INdex). *tot_num(INdex))/sum(tot_num(INdex));
save(savename,'weight_ave' , 'tot_num' , 'num_o_traj' , 'Ds_all','dmax_ind' , 'err_diff');

```

3.1. Trajectories script

```

load(matfile); %for batch script

c_index=dist_data(:,1);
n_index=dist_data(:,2);
xc=dist_data(:,5);
yc=dist_data(:,6);

```



```

dx=dist_data(:,7);
dy=dist_data(:,8);
big = size(c_index(:,1));
if big(1,1) > 1
npairs=max(max(size(xc)));
next_pair_in_chain=zeros(npairs,1);
n_connects=zeros(npairs,1);

for i=1:npairs %loop through current frames
    for j=1:npairs %loop through next frames
        if c_index(i)==n_index(j)
            n_connects(i)=n_connects(i)+1;
            n_connects(j)=n_connects(j)+1;
            next_pair_in_chain(j)=i;
            break
        end
    end
end

c_used=zeros(npairs,1);
n_traj=0;

for i=1:npairs
    if c_used(i)==0
        c_used(i)=1;
        n_traj=n_traj+1;
        trajectories(n_traj,1)=c_index(i);
        trajectories(n_traj,2)=n_index(i);
        next_i=next_pair_in_chain(i);
        column=3;
        while next_i ~= 0
            trajectories(n_traj,column)=n_index(next_i);
            c_used(next_i)=1;
            column=column+1;
            next_i=next_pair_in_chain(next_i);
        end
        traj_length(n_traj)=column-1;
    end
end
end
% figure
% set(gcf,'Name',[this_file(1:index(2)-1), ': trajectories']); %for batch
% plot(xc,yc,'.r'),axis image,hold on;
% for i=1:npairs

```

```
% if n_connects(i)>=1
% plot([xc(i) xc(i)+dx(i)],[yc(i) yc(i)+dy(i)],'Color',[0 1 0],'LineWidth',0.1);
% else
% plot([xc(i) xc(i)+dx(i)],[yc(i) yc(i)+dy(i)],'Color',[0 0 1],'LineWidth',0.1);
% end
% end
% title('Trajectories');
% hold off
```

```
save(save_name);
if exist('trajectories','var')
    clear trajectories traj_length dist_data;
end
clear xf_all yf_all nrat red_sum green_sum;
```

3.2. Trajectories analysis script

% This is a function to analyze the data created in our trajectory analysis

% program

% Created 5/1/14 AJN

```
function[Ds_all_ave, num_con, dmax] = trajectory_analysis_func(fpath,fname,time_per_frame)
load([fpath,'\',fname]);
clear i j
xf_um=xf_all*q;
yf_um=yf_all*q;
xmin=0;
xmax=500;
ymin=0;
ymax=500;
if exist('trajectories','var')
for i=1: numel(trajectories(:,1)) %cycles through each row of the trajectories
    nt=numel(trajectories(i,trajectories(i,:)>0)); %Cycles through all nonzero columns
    xset=xf_um(trajectories(i,1:nt));
```

```

yset=yf_um(trajectories(i,1:nt));
if xset(1)>xmin && xset(1)<xmax && yset(1)>ymin && yset(1)<ymin
    xdisp=diff(xset);          % Creates a vector of differences in x values
    ydisp=diff(yset);          % Creates a vector of differences in y values
    sd=xdisp.*xdisp+ydisp.*ydisp; % Creates a vector of distances between localizations
    msd=mean(sd);              % Average distance traveled
    Ds_all(i)=msd/(4*time_per_frame); % Diffusion Coefficient of particle

end
% waitbar(i/numel(trajectories(:,1))),);
end
Ds_all_ave = mean(Ds_all);
num_con = numel(trajectories);
else
    Ds_all_ave = 0;
    num_con = 0;
end

```

4. Matlab computer program that selects localizations that emit for three or more frames

This program was written by Shawn Brackett and me. It makes use of the output from the computer program in A.3. to produce a .mat file that selects localizations that emit for three or more frames. The number of photons emitted for each frame of these localizations as well as the distance from the center of mass are outputted this code.

```

% load() % load trajectoreies var
% load() % load toleranced data
function Trajectory_analysis_4_N_and_R_grab_sum_all_and_average(toggle)
clear all
toggle=0;

```

```

[fname1, fpath1] = uigetfile('*t13.mat');
cd(fpath1);

finfo1 = dir('*t13.mat'); %builds a file information structure that contains name of all files
with .mat ext

[fname2, fpath2] = uigetfile('*traj.mat');
cd(fpath2);

finfo2 = dir('*traj.mat'); %builds a file information structure that contains name of all files
with .mat ext


num_sets = numel(finfo1);

%keyboard;

ofname=['dataav4.mat'; 'dataav5.mat'; 'dataav6.mat'; 'dataav7.mat'; 'dataav1.mat';
'dataav2.mat'; 'dataav3.mat'; 'dataav8.mat'; 'dataav9.mat'];


for k=1:num_sets
    %func_ind_tolerance(finfo(k).name)

    load(finfo1(k).name);
    load(finfo2(k).name);
%    if (toggle == 0)
%        figure %prepares to make a figure
%        hold on %waits for the parameters to be set for the figure
%    end

    clear sumdata %clears sumdata so that this data from a previous file is not added onto the
next one

    clear rownum %clears rownum so that this data from a previous file is not added onto the
next one

    clear sumdatasum %clears sumdatasum so that this data from a previous file is not added
onto the next one

```

clear Raverage %clears Raverage so that this data from a previous file is not added onto the next one

```
m =1;
x=zeros(10,200);
y=zeros(10,200);
p=zeros(10,200);
R=zeros(10,200);
xf_mean=mean(xf_all);
yf_mean=mean(yf_all);
```

```
for i=1:size(trajectories,1) %goes through all trajectory rows in the data set and calls them i
    %keyboard;
```

```
    len1 = length(find(trajectories(i,:)));%length of find trajectories is how we define len here
```

```
    x(1:len1,m) = find(trajectories(i,:)); %defines a new variable x that finds all indices and
values of nonzero elements for the ith row
```

```
    if len1>=3 %the if statement is such that when the length of the row is more than three
(there are more than three columns with a nonzero element)
```

```
        xtemp = (xf_all(trajectories(i,x(1:len1,m))))-xf_mean)*q; %converts x positions of
localizations to microns and places them with respect to the mean value as a center of mass
frame change
```

```
        ytemp = (yf_all(trajectories(i,x(1:len1,m))))-yf_mean)*q; %converts y positions of
localizations to microns and places them with respect to the mean value as a center of mass
frame change
```

```
        Rtemp=sqrt(xtemp.*xtemp+ytemp.*ytemp); %calculates the distance between the
center of mass and a particular localization and stores this as Rtemp
```

```
        R(1:len1,m)=Rtemp; %defines a new variable R that is the distance from the center of
mass for the ith row with the corresponding indices and values of nonzero elements for said
row
```

```
        y(1:len1,m) = N(trajectories(i,x(1:len1,m)));%defines a new variable y that is the
number of photons for the ith row with the corresponding indices and values of nonzero
elements for said row
```

`p(1:len1,m) = grab_sum_all(trajectories(i,x(1:len1,m)));` %defines a new variable p that is the number photons added around and to the number for the brightest pixel of a localization for the ith row with the corresponding indices and values of nonzero elements for said row

`sumdata(m) = sum(y(2:(len1-1),m));` %defines sumdata(m) to be equal to the sum of the number of photons in y, goes from 2nd column to 2nd to last column. As a result we pick out the columns that do not involve the molecule turning on and those of the molecule turning off

`sumdatasum(m) = sum(p(2:(len1-1),m));` %defines sumdata(m) to be equal to the sum of the (photon pixel sum method) number of photons in y, goes from 2nd column to 2nd to last column. As a result we pick out the columns that do not involve the molecule turning on and those of the molecule turning off

`Raverage(m) = mean(R(2:(len1-1),m));` %defines Raverage(m) to be the average value of R in a sample

`rownum(m) = i;` %defines rownum(m) to be equal to the row number, i

`len(m) = len1;` %defines len(m) to be equal to the length of the find trajectories

`%if (toggle == 0)`

`% plot(x(1:len1,m),y(1:len1,m));` %plots x and y on a graph for the ith row

`%end`

`m = m + 1;` %m is the number of trajectories passing the greater than three frame test

`end`

`%for j=1:size(trajectories,2) %picks out all of the trajectory columns and calls them j`

`% y = zeros(1,size(trajectories,2));`

`% if trajectories(i,j)>0 && sum(trajectories(i,:)>0)>=3` %picks out all of the trajectories with row and column greater than zero as well as all of the trajectories that have greater than three columns with a value greater than 0

`%plot(j,N(trajectories(i,j)),'.') %plots j versus the number of photons for the columns and rows of respective trajectories`

`% y(j) = N(trajectories(i,j));`

`% end`

`% plot(x,y);`

```

        end
%     if (toggle == 0)
%         ylabel('photons')%this row labels the x-axis
%         xlabel('step')%this row labels the x-axis
%         title(num2str(k));
%         hold off
%         figure
%         plot(rownum,sumdata, '.');
%         ylabel('total photons')
%         xlabel('molecule')
%         title(num2str(k));
%     end

    X = x(:,1:(m-1));
    Y = y(:,1:(m-1));
    Rsaved=R(:,1:(m-1));
    psaved=p(:,1:(m-1));
    m = m-1;

    save(ofname(k,:), 'sumdata', 'rownum', 'X', 'Y', 'Rsaved', 'psaved', 'len', 'm', 'sumdatasum', 'Raverage');

% end

%data_concatanation2_grab_sum_all();

```

```
end
```

5. Concatenate multiple .mat files of the 4 output

This program was written by Shawn Brackett and me. It makes use of the output from the computer program in A.4 to produce a .mat file that combines all of the outputs in a folder

from the program aforementioned. The combined number of photons emitted for each frame of these localizations as well as the distance from the center of mass are placed in this outputted .mat file.

```
%Concatenate multiple trajectory data*.mat files together (* refers to
%number of data file) into finaldata.mat
function data_concatanation2_grab_sum_all_nip_switch()
    [fname1, fpath1] = uigetfile('data*.mat');
    cd(fpath1);
    finfo1 = dir('data*.mat'); %builds a file information structure that contains name of all files
    with .mat ext
    %keyboard
    num_sets = numel(finfo1);

    data = struct('X', {}, 'Y', {}, 'totalPcount', {}, 'rownum', {}, 'numframes', {}, 'numMol',
    {}, 'Rsaved', {}, 'psaved', {}, 'sumdatasum', {});

    for i=1:num_sets

        load(finfo1(i).name);
        data(i).X = X;
        data(i).Y = Y;
        data(i).Rsaved = Rsaved;
        data(i).psaved = psaved;
        data(i).totalPcount = sumdata;
        data(i).rownum = rownum;
        data(i).numframes = len;
        data(i).numMol = m;
        data(i).Rreal = Raverage;
        data(i).preal = sumdatasum; % check whether this is correct
    end
    save('finaldatanipswitchcross.mat','data');
    %keyboard;
end
```

6. Matlab program: graphs, fits experimental data photon number histograms

This program was written by Shawn Brackett and me. It takes the outputted .mat file from A.5, and produces number of photon histograms with fitted functions to said histograms.

```
%loading experimental data
```

```
clear all
```



```

%close all

load('finaldatanipswitchcross.mat');
num_sets = numel(data);
k=1:6;
spot = 1;
for j = 1:num_sets
    %figure
    %keyboard
    for i = 1:(data(j).numMol)
        %hold on
        %plot(data(j).X(1:data(j).numframes(i),i),data(j).Y(1:data(j).numframes(i),i))
        tmpRsaved = data(j).Rsaved(2:(data(j).numframes(i)-1),i);
        Rsaved(spot:(spot+length(tmpRsaved)-1)) = tmpRsaved';
        tmppsaved = data(j).psaved(2:(data(j).numframes(i)-1),i);
        psaved(spot:(spot+length(tmppsaved)-1)) = tmppsaved';
        tmpY = data(j).Y(2:(data(j).numframes(i)-1),i);
        Y(spot:(spot+length(tmpY)-1)) = tmpY';
        spot = spot + length(tmpY);
        x(k) = k;
        y1(k) = data(j).totalPcount(i);
        y2(k) = data(j).numframes(i);
        R(k)=data(j).Rreal(i);
        p(k)=data(j).preal(i);
        k=k+1;
    end
    %keyboard
end
A=1450000;

```

```

x0=5.0;
r0=0.85;

figure
bins=(13:(987/87.5):1000);
%bins = (0:0.2:10);
[n, xout]=hist((Y(Y>13 & Y<1000)), bins);
bar(xout,n)
%ylim([0 7000]);
%plot(bins,[n,xout]);
hold on;

% m = mean(1045500*(1/(sqrt(2*pi)))*(1./xout)*(1/0.63835).*exp(-0.5*(log(xout)-
5.0452).*(log(xout)-5.0452)/(2*0.63835*0.63835)));

% v = var(1045500*(1/(sqrt(2*pi)))*(1./xout)*(1/0.63835).*exp(-0.5*(log(xout)-
5.0452).*(log(xout)-5.0452)/(2*0.63835*0.63835)));

% %ylim([0 1400])
% % [c,i]=max(n);
% % xout(i)

title(['Experimental crossbeam histogram and fitted function']);
ylabel('Events');
xlabel('Photons');

beta0 = [A, r0, x0];
[beta,R,J,CovB,MSE] =
nlinfit(xout,n,@nlinfit_log_dist_of_simulation_crossbeam_Gaussian_area_all_fram,beta0);
ci=nlparci(beta,R,'covar',CovB);%pops out a matrix that shows with a 95% confidence interval
what values are the maximum and minimum for beta(1), beta(2) and beta(3)

% %try to plot experimental data with the fitted function
xh=[13:1:800];
alpha(1) = ((ci(1,1)+ci(1,2))/2);

```

```

P = alpha(1)*(1/(sqrt(2*pi)))*(1./xh)*(1/((ci(2,1)+ci(2,2))/2)).*exp(-(log(xh)-
((ci(3,1)+ci(3,2))/2)).*(log(xh)-((ci(3,1)+ci(3,2))/2))/(2*((ci(2,1)+ci(2,2))/2)^2));

IP = ci(1,2)*(1/(sqrt(2*pi)))*(1./xh)*(1/ci(2,2)).*exp(-(log(xh)-ci(3,2)).*(log(xh)-
ci(3,2))/(2*ci(2,2)^2));

sP = ci(1,1)*(1/(sqrt(2*pi)))*(1./xh)*(1/ci(2,1)).*exp(-(log(xh)-ci(3,1)).*(log(xh)-
ci(3,1))/(2*ci(2,1)^2));

plot(xh,P,'color','b','LineWidth',1);
plot(xh,sP,'color','m','LineWidth',1);
plot(xh,IP,'color','g','LineWidth',1);

xlim([0 500]);

%ylim([0 450]);

```

7. Matlab simulation program of cross-beam vs. widefield number of photon histograms

This program was written by Dr. Sam T. Hess and me. It simulates a data set and outputs a number of photon histogram for certain numbers of molecules, beam powers, beam sizes and imaging areas, particularly for two circularly polarized excitation beams incident onto a sample.

```

clear all

close all

np=20225;      % total number of molecules to simulate

% begin section defining a uniform distribution of molecular transition dipole orientations
dtheta=0.001;

thetaval=0:dtheta:pi;
ptheta=sin(thetaval);
intptheta=0.5*(1-cos(thetaval));
%plot(thetaval,intptheta);

for i=1:np
    s=rand;
    ind=find(intptheta>s,1,'first');

```

```

    theta(i)=thetaval(ind);
end
theta=theta';
%theta=rand(np,1)*pi;

phi=rand(np,1)*2*pi; %picking positions for particles
xp=sin(theta).*cos(phi);
yp=sin(theta).*sin(phi);
zp=cos(theta);

% end of section defining a uniform distribution of molecular transition dipole orientations


Xp=rand(np,1); %100*0.133;
Yp=rand(np,1); %100*0.133;

rp=4.5*(Xp.*Xp+Yp.*Yp).^(0.5); % radius for particles from center of field (beam profile), in
microns

PmW=4.36; % mW at 561 nm                % power at the sample, in milliwatts
PmW532= 5.1; % mW at 532

beamR=10.4; % microns for 561
beamR532=11.4; % microns

beam_area=beamR*beamR*pi/2; % microns squared

```

```

beam_area_cm2=beam_area*1e-8;

beam_area532=beamR532*beamR532*pi/2; % microns squared
beam_area532_cm2=beam_area532*1e-8;

I0=PmW*1e-3/(beam_area_cm2);    % watts/cm2;
I0532=PmW532*1e-3/(beam_area532_cm2);    % watts/cm2;

wavel=561;
energy_per_photon_eV=197.3*2*pi/wavel;
energy_per_photon_J=energy_per_photon_eV*1.602e-19;

wavel532=532;
energy_per_photon_eV532=197.3*2*pi/wavel532;
energy_per_photon_J532=energy_per_photon_eV532*1.602e-19;

I0_phot=I0/energy_per_photon_J;
ExtCoeff=28560;    % extinction coefficient of Dendra2 at 561 nm
cross_sec=ExtCoeff*3.82e-21; % cm2
kx0=I0_phot*cross_sec*exp(-2*rp.*rp/(beamR*beamR));    % 561 excitation rate (max)


I0_phot532=I0532/energy_per_photon_J532;
ExtCoeff532=21308;    % extinction coefficient of Dendra2 at 532 nm
cross_sec532=ExtCoeff532*3.82e-21; % cm2
kx1=I0_phot532*cross_sec532*exp(-2*rp.*rp/(beamR532*beamR532));    % 532 excitation
rate (max)

```

```
%kx1=kx0*3;          % 532 excitation rate (max) --- change this to affect the excitation rate
of the 532 relative to the 561
```

```
%kx0=0;
```

```
    alphadeg=0; %(i-1)*20;          % alpha is the angle between the 561 beam and the 532 nm
beam (0 is widefield, 90 is fully crossed beam)
```

```
    alpha=alphadeg*pi/180;          % alpha value in radians
```

```
    kx=kx0.*sin(theta).sin(theta)+kx1.*sin(theta+alpha).sin(theta+alpha); % circularly polarized
excitation in the xy plane
```

```
    time_per_frame=0.0095;          % seconds
```

```
    QY=0.55;          % quantum yield
```

```
    DE=0.020;          % detection efficiency
```

```
% phiB=2e-5;          % photobleaching yield (not used except in Nmax calculations)
```

```
% Nmax=1/phiB*QY*DE;
```

```
    N=kx*QY*time_per_frame*DE;      % number of detected photons per frame (i.e. the middle
frame only)
```

```
    %N=Nmax*double((N>Nmax))+N.*double(N<=Nmax);
```

```
    figure
```

```
    %bins=(0:10:2000);
```

```
    %bins1=(0:10:2000);
```

```
    bins=(0:11.28:1000);
```

```
    bins1=(0:11.28:1000);
```

```
    %bins = (0:0.2:10);
```

```
    %[n, xout]=hist((Y(Y>13 & Y<5000)), bins);
```

```
    %bar(xout,n)
```

```
    %ylim([0 7000]);
```

```
    %plot(bins,[n,xout]);
```

```

hold on;

[m, yout]=hist(N(N>13 & N<1000),bins1);

plot(yout,m,'color','r','LineWidth',2);

%plot(bins1,nhist,'color','r');

%bar(bins,nhist);

xlim([0 200]);

ylim([0 6000]);

hold on;

xlabel('Photons');

ylabel('Events');

title('Cross-beam simulation with fitted functions');


A=2050000;

x0=4;

r0=1.5;

beta0 = [A, r0, x0];

[beta,R,J,CovB,MSE] =
nlinfit(yout,m,@nlinfit_log_dist_of_simulation_crossbeam_Gaussian_area_all_fram,beta0);

ci=nlparci(beta,R,'covar',CovB);%pops out a matrix that shows with a 95% confidence interval
what values are the maximum and minimum for beta(1), beta(2) and beta(3)

% %try to plot experimental data with the fitted function

xh=[0:1:200];

alpha(1) = ((ci(1,1)+ci(1,2))/2);

P = alpha(1)*(1/(sqrt(2*pi)))*(1./xh)*(1/((ci(2,1)+ci(2,2))/2)).*exp(-(log(xh)-
((ci(3,1)+ci(3,2))/2)).*(log(xh)-((ci(3,1)+ci(3,2))/2))/(2*((ci(2,1)+ci(2,2))/2)^2));

IP = ci(1,2)*(1/(sqrt(2*pi)))*(1./xh)*(1/ci(2,2)).*exp(-(log(xh)-ci(3,2)).*(log(xh)-
ci(3,2))/(2*ci(2,2)^2));

sP = ci(1,1)*(1/(sqrt(2*pi)))*(1./xh)*(1/ci(2,1)).*exp(-(log(xh)-ci(3,1)).*(log(xh)-
ci(3,1))/(2*ci(2,1)^2));

plot(xh,P,'color','b','LineWidth',1);

```

```
plot(xh,sP,'color','m','LineWidth',1);
plot(xh,lP,'color','g','LineWidth',1);
```

8. Examples of single cell Gaussian area and Photon pixel sum histograms

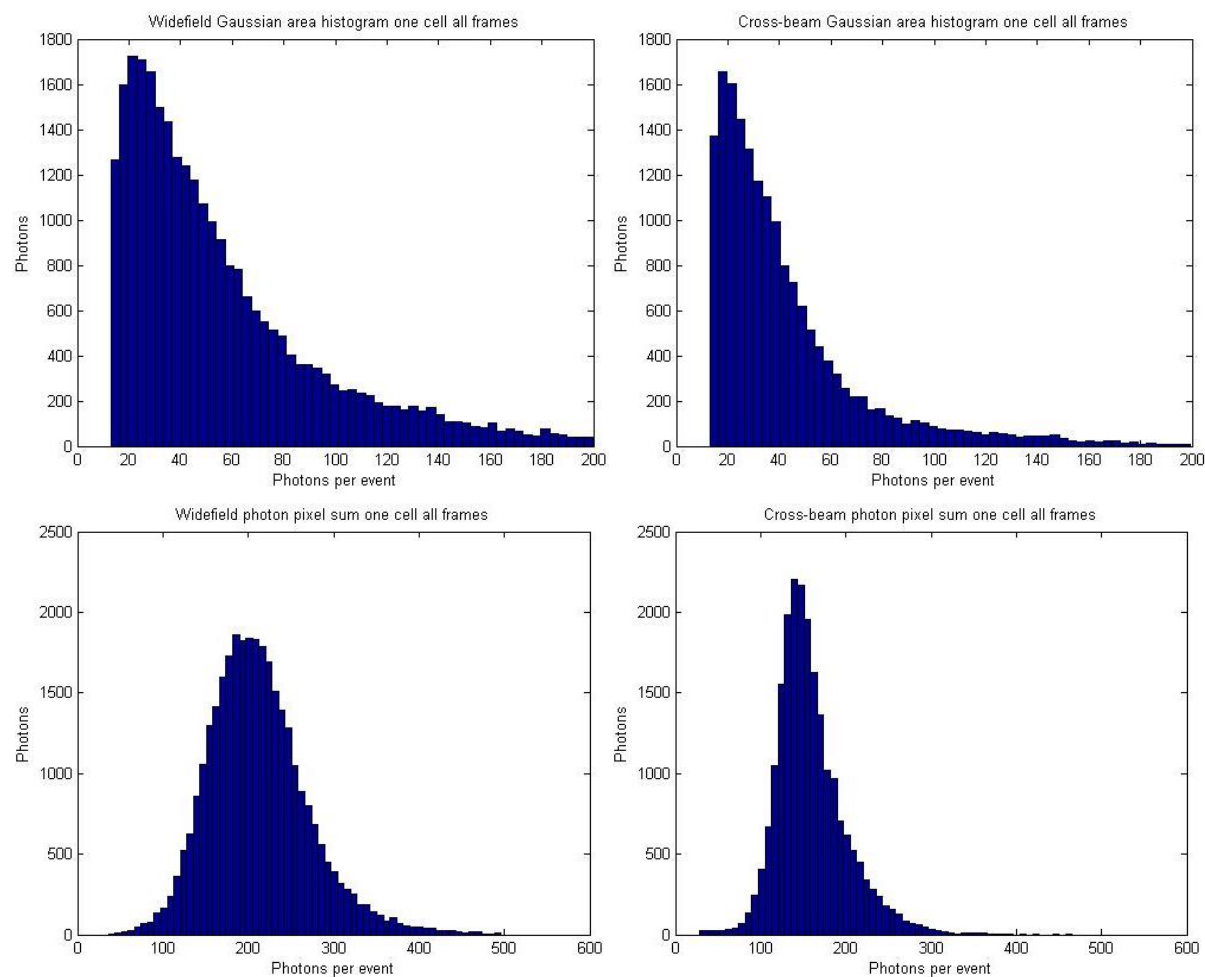


Figure A.1: Single cell photon histograms. The top histograms above show number of photons per localization per frame, while the two bottom histograms show their corresponding photon pixel-sum histograms. The histograms on the left are for one cell in widefield illumination, while those on the right are for another in cross-beam illumination. These are examples of single cell data sets that were used with others to make figures 3.4 and 3.5. The cross-beam illumination, for these two cells, had fewer localizations and less wide histograms.

BIOGRAPHY OF THE AUTHOR

Matthew Valles graduated from Barrington High School of Rhode Island, in 2009, and obtained a Bachelor's in Science from Bates College in 2013. Matthew is a candidate for the Masters of Science in Physics from the University of Maine in May 2017.